Bioconjugate Chemistry

Article

pubs.acs.org/bc

Red Emitting Neutral Fluorescent Glycoconjugates for Membrane Optical Imaging

Sébastien Redon,[†,¶] Julien Massin,[‡] Sandrine Pouvreau,[§] Evelien De Meulenaere,[∥,⊥] Koen Clays,[∥] Yves Queneau,[†,¶] Chantal Andraud,[‡] Agnès Girard-Egrot,[#,¶] Yann Bretonnière,*[,‡] and Stéphane Chambert*[,†,¶]

[†]Laboratoire de Chimie Organique et Bioorganique, ICBMS, INSA Lyon, Bât. J. Verne, 20 Avenue A. Einstein, 69621 Villeurbanne Cedex, France

[¶]Institut de Chimie et de Biochimie Moléculaires et Supramoléculaires, CNRS UMR 5246, Université de Lyon, Université Lyon 1, INSA-Lyon, CPE-Lyon, Bât. Curien, 43 Bd du 11 Novembre 1918, 69622 Villeurbanne, France

[‡]Laboratoire de Chimie de l'ENS de Lyon, Université de Lyon, CNRS UMR 5182, Université Lyon 1, ENS de Lyon, 46 allée d'Italie, 69364 Lyon Cedex, France

[§]Physiologie Intégrative, Cellulaire et Moléculaire, Université Lyon 1, CNRS UMR 5123, 60622, Villeurbanne, France

[∥]Laboratory for Molecular Electronics and Photonics, KULeuven, Celestijnenlaan 200D box 2425, 3001 Heverlee, Belgium

[⊥]Centre of Microbial and Plant Genetics, KULeuven, G. Geenslaan 1 box 2471, 3001 Heverlee, Belgium

[#]Laboratoire de Génie Enzymatique, Membranes Biomimétiques et Assemblages Supramoléculaires, Institut de Chimie et de Biochimie Moléculaires et Supramoléculaires, ICBMS, Université Lyon 1, Bât. Curien, 43 Bd du 11 Novembre 1918, 69622 Villeurbanne, France

S *Supporting Information*

ABSTRACT: A family of neutral fluorescent probes was developed, mimicking the overall structure of natural glycolipids in order to optimize their membrane affinity. Nonreducing commercially available di- or trisaccharidic structures were connected to a push−pull chromophore based on dicyanoisophorone electron-accepting group, which proved to fluoresce in the red region with a very large Stokes shift. This straightforward synthetic strategy brought structural variations to a series of probes, which were studied for their optical, biophysical, and biological properties. The insertion properties of the different probes into membranes were evaluated on a model system using the Langmuir monolayer balance technique. Confocal fluorescence microscopy performed on muscle cells showed completely different localizations and loading efficiencies depending on the structure of the probes. When compared to the commercially available ANEPPS, a family of commonly used membrane imaging dyes, the most efficient probes showed a similar brightness, but a sharper pattern was observed. According to this study, compounds bearing one chromophore, a limited size of the carbohydrate moiety, and an overall rod-like shape gave the best results.

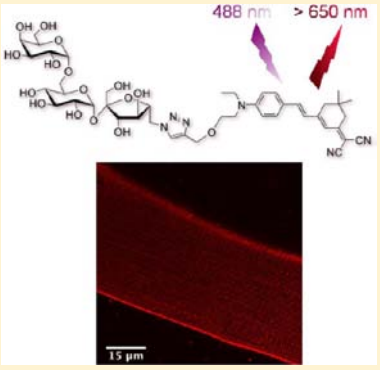

■ INTRODUCTION

In the past decades, the use of small fluorescent molecules as specific probes for fluorescence imaging led to biochemical, biological, diagnostic, or therapeutic applications.[1] While a large portion of the dyes available today are still derived from a limited number of different fluorophores,[2] the search for new chemical structures or building blocks, sometimes mimicking nature, may lead to improved imaging opportunities to study fundamental biochemistry, and some of those new products may even find their way to medical applications. Membrane probes, especially designed for targeting eukaryotic cell membranes, have been used to monitor biological processes both in membrane models and in cellular experiments. Membrane probes are useful reporters of events happening at the molecular level in or near the cell membrane, including visualization and measurements of the membrane potential.[3] In general, these membrane probes mostly rely on charged or zwitterionic aromatic structures, such as carbocyanines, oxonols, fluoresceins, or rhodamines. The commercially available and very popular ANEP (amino naphthyl ethynyl pyridinium) derivatives also belong to this category.[4] Neutral compounds such as Laurdan or Prodan have also been employed,[5−7] but they are very lipophilic and require excitation by UV wavelengths. Because toxicity and localization seem to be fundamental difficulties encountered with several existing membrane probes,[8−11] our goal is to design, synthesize, and study neutral probes with reduced toxicity. Our design is based on the association of a carbohydrate structure with a push−pull

Received: January 31, 2014
Published: February 14, 2014

   dx.doi.org/10.1021/bc500047r | *Bioconjugate Chem.* 2014, 25, 773−787

fluorophore. By mimicking the overall structure of natural glycolipids we wish to benefit from their well-known membrane specificity[12] in order to produce new fluorescent tools for membrane imaging. Using a similar approach, conjugation of a fluorescent tag to a trisaccharide heterobifunctional linker connected to a cholesterol moiety was reported to incorporate into cell surfaces enriched in microdomains.[13] However, in our approach, the uncharged lipophilic fluorophore is designed to be located in the membrane while the carbohydrate moiety would influence the orientation inside the membrane, eventually keeping the probe in the outer leaflet of the membrane. This is a key property for performing second-order nonlinear optical experiments such as second-harmonic imaging (SHIM).[14−16]

In a previous study, we reported the synthesis of a series of neoglycolipidic membrane probes that were the result of the association of a glucose or lactose scaffold onto a conjugated push−pull fluorophore.[17] This fluorophore itself was based on a pyridine dicarboxamide acceptor group, a fluorenethynyl π-conjugated bridge, and a dialkylamino donor with lipophilic alkyl chain substitutes of varying length. This fluorophore/carbohydrate association has proven to be valuable for efficiently targeting the cell membrane and even showed potential for its use in nonlinear optical imaging methods. However, these probes suffered from poor water solubility. In an effort to obtain dyes suitable for the imaging of isolated cells and ultimately *in situ*, a number of desired properties was defined: (i) good water solubility allowing a maximum final concentration of 1:1000 of DMSO in the biological medium, (ii) good membrane specificity, (iii) low background fluorescence due to unspecific labeling, (iv) extended (over two hours) membrane staining, (v) the ability to report events happening at the membrane surface, and (vi) reduced cytotoxicity and phototoxicity. This was nicely exemplified with the development of new fluorescent probes based on 3-hydroxyflavone derivatives whose emission was highly sensitive to the lipid composition of the biomembranes and could probe the spatial distribution of the apoptotic changes at the cell plasma membranes.[18] As other examples, C-laurdan or S-laurdan derivatives specially designed for two-photon microscopy showed brighter two-photon fluorescence than classically used laurdan and reflected the cell environment more accurately.[19,20] The great sensitivity of the emission to the membrane polarity enabled visualization of lipid rafts and membrane organization. Biological imaging favors fluorescent dyes with spectral properties in the red region essentially because measurements at these wavelengths suffer less from light scattering and absorption by the sample, resulting in reduced heating of the cell, as well as a reduced background signal originating from autofluorescence. A Nile Red derivative showing a red-shifted emission combined with reduced flip-flop in the membrane was reported to offer considerable advantage compared to existing probes for studying cholesterol and lipid order in biomembranes.[21] Additionally, dyes presenting a large Stokes shift are interesting in the perspective of multicolor imaging as they can add a supplementary color and allow the simultaneous acquisition of signals from several dyes using a single excitation wavelength.[22]

In this work, we wish to extend the use of fluorescent glycoprobes for membrane imaging and progress toward a better understanding of the molecular requirement ensuring the appropriate loading and biological activity of such probes. To this end, relatively small push−pull chromophore alkynes were attached to different azidocarbohydrate entities using the established Huisgen copper(I) catalyzed cycloaddition. Using the same fluorophore, the structural variations on the different probes are only brought by the size and structure of their carbohydrate moieties. The membrane insertion properties of the new series of probes have been studied using a membrane monolayer model technique and directly evaluated in a biological context by confocal imaging on isolated skeletal muscle cells (muscle fibers) from mouse.

RESULTS AND DISCUSSION

Probes Design. For this study, a red emitting push−pull chromophore based on the dicyanoisophorone electron-accepting group and having a relatively small size for attaining the suitable water solubility of the final probes was selected. This structure, originally developed by Lemke,[25] displayed a very large Stokes shift and, due to its push−pull nature, a strong environmentally sensitive response of its fluorescence was demonstrated.[26,27] Interestingly, the fluorescence quantum yield was shown to increase in viscous media[26,27] making this particular fluorophore very attractive for media with restrictive fluidity such as cell membrane. The hydrophilicity of the probes was introduced by grafting different carbohydrate entities onto the fluorophores. The intrinsic nonionic nature of carbohydrates was chosen because they are less likely to modify the local charges present at the surface of the cells. We also wished to use carbohydrate structures different from the ones naturally occurring on glycolipids such as gangliosides in order to minimize the possible interference with their biological processing (e.g., enzymatic hydrolysis or recognition by lectins). The 1,2,3-triazole linker between the fluorophore and the carbohydrates was selected for its biocompatibility[28,29] and its formation via the convenient Huisgen copper(I) catalyzed cyclization.[30,31]

Synthesis of the Alkyne Fluorophores. For connecting the carbohydrate moieties to the chromophore, modified versions of the same push−pull chromophore bearing either one or two terminal alkyne functions were synthesized in high yields using a three-step procedure (Scheme 1). 2-(*N*-Ethylanilino)ethanol **1a** or *N*-phenyldiethanolamine **1b** were first alkylated by propargyl bromide to give the corresponding propargyl ethers **2a** and **2b**. They were then transformed by a Vilsmeier−Haack reaction into their corresponding counterparts **3a** and **3b**, bearing aldehyde functions in position 4 of the aniline rings. After a Knoevenagel reaction with the known dicyano compound **4**, [26] the aldehydes furnished the desired conjugated fluorophores **5a** and **5b** in very good yields.

Synthesis of Azidocarbohydrates. Four different commercially available nonreducing di- or trisaccharides were selected: sucrose **6a** and trehalose **7a** for the disaccharidic structures; raffinose **8a** and melezitose **9a** for the linear or branched trisaccharides, respectively (Scheme 2). Sucrose was selected for its well-known very high solubility in water, raffinose and melezitose being commercially available trisaccharides bearing a sucrose scaffold. We used the direct azidation method under Mitsunobu conditions developed by our group for regioselectively introducing the desired azido groups without the need for intermediate protection/deprotection protocols.[23] Briefly, an HN_3 solution was first produced by reacting NaN_3 with H_2SO_4 in toluene. The resulting solution 5% HN_3/toluene was dried and used directly in excess. The stoichiometry of reactions was controlled by the quantity of PPh_3/DIAD added. After dichloromethane extraction and column chromatography, the monoazido-sucrose **6b** and diazido-trehalose **7b**, as well as

dx.doi.org/10.1021/bc500047r | *Bioconjugate Chem.* 2014, 25, 773−787

Scheme 1. Synthesis of Propargyl Ether Fluorophores 5a and 5b[a]

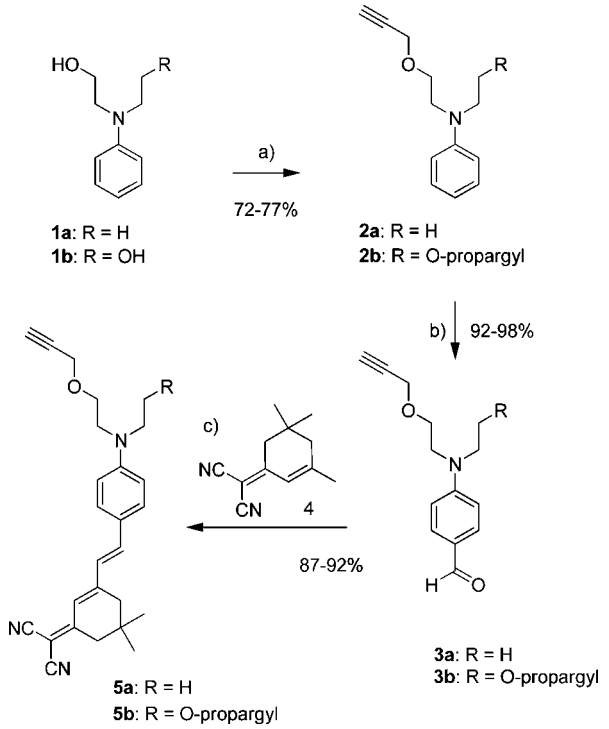

[a](a) Propargyl bromide (80% in toluene), NaH, DMF, 0 to 20 °C overnight; (b) $POCl_3$, DMF, 0 to 50 °C, overnight; (c) 2-(3,5,5-trimethylcyclohex-2-enylidene)malononitrile **4**, MeCN, piperidine, 20 °C, overnight.

Scheme 2. Synthesis of Azidoglycosides 6b−9b[23a]

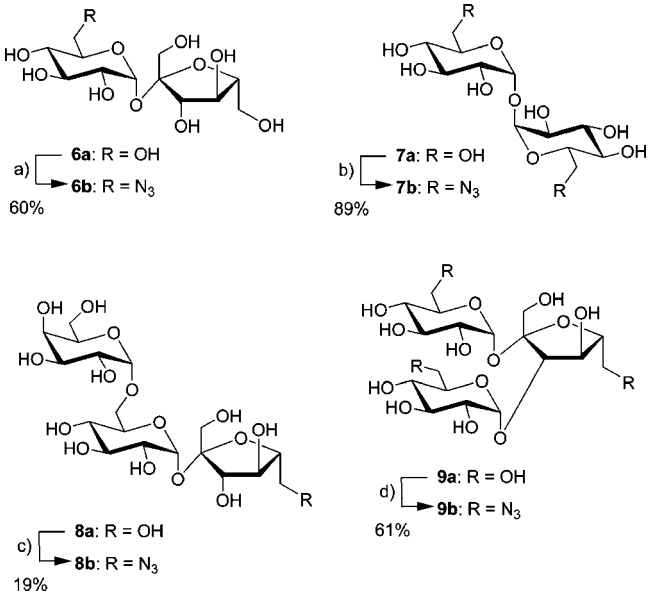

[a](a) Excess HN_3, 2 equiv. PPh_3/DIAD, DMF, 0 to 20 °C overnight; (b), (c), and (d) excess HN_3, 5 equiv. PPh_3/DIAD, DMF, 0 to 20 °C overnight.

the monoazido-raffinose **8b** and triazido-melezitose, were isolated in moderate to good yield (19%−89%).

In order to obtain a branched monoazido-trisaccharide, we took advantage of the relative reactivity of the primary hydroxyl groups of melezitose under Mitsunobu conditions (Scheme 3). In a first step, the 6 and 6″ positions of the glucose residues were

Scheme 3. Synthesis of 6′-Azidomelezitose 12b[a]

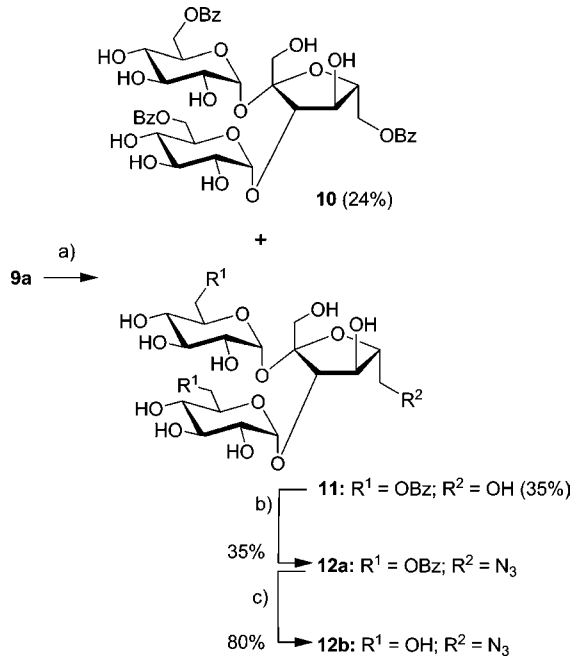

[a](a) $PhCO_2H$ (4 equiv), DIAD (4 equiv), PPh_3 (4 equiv), DMF, 0 to 20 °C overnight; (b) excess HN_3, 5 equiv PPh_3/DIAD, DMF, 0 to 20 °C overnight; (c) KOH (1 M in water, 4 equiv), MeOH, 20 °C, 1 h.

benzoylated, and the reaction was carried out in DMF using 4 equiv of PPh_3, DIAD, and benzoic acid to give triester **10** and the diester **11** in 32% and 24% yield, respectively. The diester **11** was subsequently treated in a second Mitsunobu reaction with excess of HN_3/toluene and 5 equiv of PPh_3/DIAD to give the monoazido-melezitose diester **12a** in a moderate 35% yield. Finally, the cleavage of benzoate esters cleavage gave the desired 6′-azidomelezitose **12b** in 80% yield.

Synthesis of the Probes. With both the alkyne fluorophores and the azidocarbohydrates in hand, the assembly of the probes was achieved. Two main problems were encountered during the coupling reaction: the very different nature of the two components involved in terms of polarity required first to tune the solvent system employed to a chloroform/methanol mixture and to increase the reaction temperature (almost no product was observed by TLC after 14 h at 20 °C). Due to the relative sensitivity of the fluorophore to basic conditions, certain click conditions (e.g., the one involving the use of tertiary amines) were inappropriate. The first condition we used (method A) involved the use of copper iodide at 65 °C for 14 h giving moderate to low yields (25−65%) and was found particularly ineffective when the reaction involved polyazido-carbohydrates (Scheme 4). To overcome this problem, a second procedure (method B), involving microwave irradiation[32,33] and an organic soluble catalyst ($CuI•P(OEt)_3$)[34] significantly increased the yields (55−90%) and decreased the reaction time. This method was effectively performed on di- and triazidocarbohydrates for grafting several fluorophores simultaneously (Scheme 4).

These syntheses provided us with a series of new carbohydrate probes bearing variations on the size and structure of the carbohydrate moieties. The linear disaccharidic (**13**) and

dx.doi.org/10.1021/bc500047r | Bioconjugate Chem. 2014, 25, 773−787

Scheme 4. Synthesis of Probes 13−19[a]

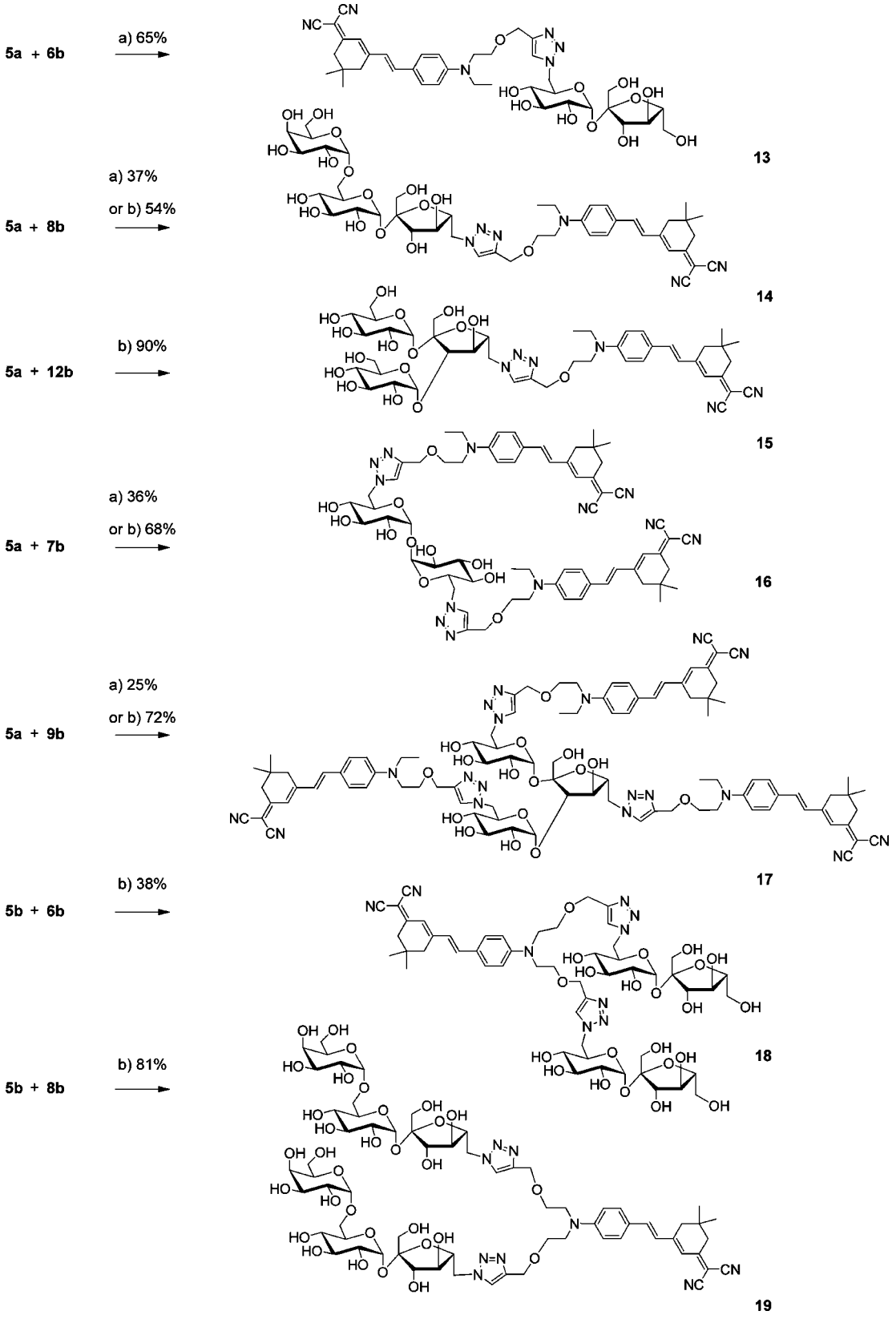

[a](a) Method A: CuI, $CHCl_3$/MeOH, 65 °C, 14 h; (b) Method B: CuI•$P(OEt)_3$, $CHCl_3$/MeOH, MW, 100 °C, 3 h.

trisaccharidic (**14**) structures were complemented by a branched trisaccharidic one (**15**). Two structures with a 1:1 carbohydrate to fluorophore ratio, bearing two (**16**) or three (**17**) fluorophores were obtained. Finally, the structures containing four (**18**) and six (**19**) glycosides, respectively, gave molecules with the strongest polarity.

dx.doi.org/10.1021/bc500047r | *Bioconjugate Chem.* 2014, 25, 773−787

Optical Characterization of the Probes. The optical properties of the probes **13**–**19** were measured in water or in a methanol–water mixture (5/1) for the less soluble compounds (**16**–**17**). A representative example of their normalized absorption and emission spectra is given for probe **13** (Figure 1). The absorption spectra do not vary significantly from one

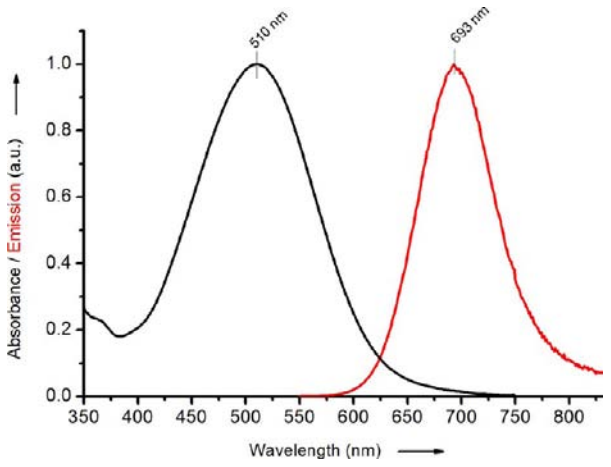

Figure 1. Normalized absorption (black) and emission (red) spectra of probe **13** in water.

compound to another, exhibiting a broad absorption band with maxima centered near 505 nm (from 501 nm for **19** to 510 nm for **13**) characteristic of the charge transfer transition from the donor to the acceptor (Table 1). The molar absorption

Table 1. Optical Properties of Probes 13–19 and Octanol–Water Partition Coefficient

Probe	λ_{abs} (ε) nm ($L.mol^{-1}.cm^{-1}$)	λ_{em} nm	$\Delta\nu$ cm^{-1}	Φ^d	$\varepsilon.\Phi$ $L.mol^{-1}.cm^{-1}$	Log P
13[a]	510 (34 500)	693	5294	0.04	1380	1.4
14[a]	508 (27 000)	692	5234	0.05	1350	0.9
15[a]	503 (26 000)	694	5471	0.05	1300	1.1
16[b]	509 (67 500[c])	685	5048	0.06	4050	n/a
17[b]	507 (88 500[c])	682	5061	0.06	5310	n/a
18[a]	505 (30 500)	695	5413	0.04	1220	−1.0
19[a]	501 (28 500)	685	5362	0.11	3135	n/a

[a]In water. [b]In methanol–water. [c]In MeOH. [d]Using erythrosine B as reference (Φ = 0.09 in water).

coefficients on the other hand increase from 26 000 $L.mol^{-1}.cm^{-1}$ for compound **15** with one chromophore moiety to 67 500 $L.mol^{-1}.cm^{-1}$ for compound **16** and 88 500 $L.mol^{-1}.cm^{-1}$ for compound **17** bearing 2 and 3 chromophores, respectively. After excitation in the charge transfer band, a bright red fluorescence was observed. The broad emission presents a very large Stokes shift ($\Delta\nu$) of nearly 5480 cm^{-1} (200 nm). The maxima of emission range from 682 nm for **17** to 695 nm for **18**. The emission quantum yields in water are on the order of 5% for all compounds with the remarkable exception of compound **19** which presents a quantum yield of 11% in water. This gives rise to far-red emitting probes displaying very interesting brightness ($\varepsilon.\Phi$) much above 1000, combined with a large Stokes shift. The presence of multiple chromophores on the same sugar slightly quenches the fluorescence, but considerably enhances the brightness.

Measurement of Octanol–Water Partition Coefficient. The Log P values were determined by measuring the fluorescence ratio obtained in each phase for every dye.[35] The values not only showed a direct correlation between the sizes of the carbohydrate moieties when compared to the overall probes, but also an effect of the nature of the carbohydrate used. Thus a large difference was observed between the disaccharidic probe **13** (Log P = 1.4), the linear (**14**, Log P = 0.9) or branched (**15**, Log P = 1.1) trisaccharidic dyes, and the tetrasaccharidic molecule **18** (Log P = −1.0). The structures bearing multiple chromophores or large sugar moieties were found either too lipophilic (**16**, **17**) or too hydrophilic (**19**) for their Log P to be efficiently determined by this method.

Membrane Insertion Ability of Glycolipidic Probes in Langmuir Monolayer. In order to evaluate the membrane insertion properties of the synthesized carbohydrate probes and in particular the effect of the amphiphilic balance of the molecular structure on their membrane activity, we used a Langmuir monolayer as an *in vitro* model of lipid membranes formed of 1-palmitoyl-2-oleoyl-*sn*-glycero-3-phosphocholine (POPC), one of the major components of the plasma membrane. This model was previously used to analyze the membrane insertion ability of carbohydrate-based probes.[36] In this model, as the experiments are performed at constant surface area, the probe-phospholipid monolayer interactions result in a time-dependent increase of the surface pressure. The penetration kinetics (i.e., surface pressure–time isotherms) recorded upon probe injection are presented in Figure 2. A large difference in the initial velocity of surface

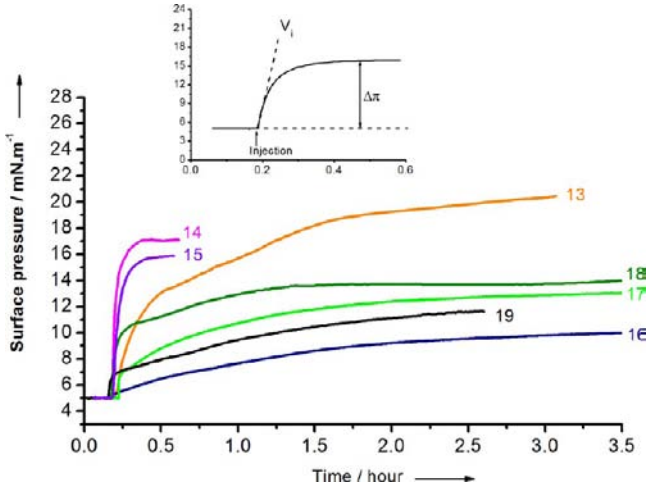

Figure 2. Surface pressure–time isotherms after injection of carbohydrate probes **13**–**19** into the subphase underneath POPC monolayer compressed at a surface pressure of 5 mN/m. $\Delta\pi$ was taken to be the difference between the initial surface pressure (π_i = 5 mN/m) and the maximal value (π_{max}) observed at plateau after insertion of the probe into the lipid monolayer. The initial velocity of surface pressure increase (V_i) was calculated as the slope of the curve ($\Delta\pi/\Delta t$) at time of probe addition (t_0).

pressure increase (V_i), and the final increase of surface pressure (π_{max}), were obtained between the different carbohydrate probes.

Small surface pressure variation indicates a nonspecific lipid monolayer interaction.[37,38] Initial experiments performed with a slightly compressed monolayer, i.e., with a low lipid packing density, give an indication of the capacity of the probe to insert into the membrane and allow discrimination between the probes. The hydrophobic probes **16** and **17** with two and three

dx.doi.org/10.1021/bc500047r | *Bioconjugate Chem.* 2014, 25, 773–787

chromophores, respectively, revealed a very slow penetration into the monolayer. The insertion was only complete after 3−4 h and the final surface pressure values reached 10.0−12.5 mN/m, leading to a low $\Delta\pi$ value of 5.0−7.5 mN/m. This behavior can probably be related to the lower solubility in water leading to aggregation, hence limiting the binding to the monolayer and delaying the insertion.[39] Hydrophilic probes **18** and **19**, bearing four and six carbohydrate units per fluorophore, exhibited two rates for penetration, a fast initial rate and a slow second process, that lead to the final equilibrium after 1.5 h or 2 h, respectively, with a $\Delta\pi$ value between 9.0 and 6.6 mN/m. The largest values of $\Delta\pi$ were obtained for probes in which the amphiphilic balance is equilibrated. For instance, probes bearing one chromophore for either a linear trisaccharide (probe **14**) or a ramified trisaccharide (probe **15**) gave rise to a faster insertion complete within 20−30 min, and a higher $\Delta\pi$ value of 11−12 mN/m. The most important insertion was achieved for probe **13**, bearing only one disaccharide moiety with a final $\Delta\pi$ value equal to 16 mN/m. However, probe **13** exhibited slower penetration kinetics. The insertion was faster for probes **14** and **15** than probe **13**. This behavior can be interpreted in terms of equilibrated hydrophilic−lipophilic balance (HLB) of probes **14** and **15**, reflected by their Log P values.

Figure 3 reports on the increase in surface pressure ($\Delta\pi$) versus the initial surface pressure (π_i) of a preformed POPC

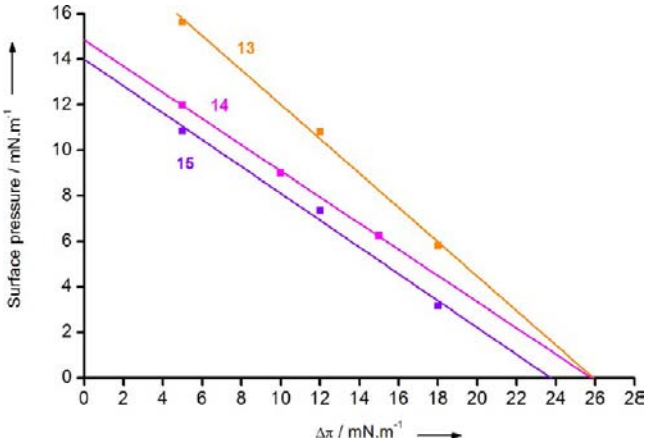

Figure 3. Plot of maximal surface pressure variation ($\Delta\pi$) versus initial surface pressure (π_i). Maximal insertion pressure (MIP) was determined from the abscissa intercept.

monolayer for the three probes **13**, **14**, **15**. As expected, an inverse correlation between the initial surface pressure (π_i) and the maximum pressure increase ($\Delta\pi$) after probe addition was observed. Higher initial monolayer surface pressures correlated with higher lipid packing densities, and consequently reduced penetration capacity of the probe.[40] Such an influence of the initial monolayer packing density on the molecular penetration demonstrates a direct probe/phospholipid interaction, as established for several other lipids and ligands.[41−43] Extrapolation of the linear relationship for $\Delta\pi$ = 0 mN/m gave the maximal insertion pressure (MIP) corresponding to the surface pressure from which insertion is no longer possible, reported in Table 2. For probe **13** a MIP value of 25.9 mN/m was found, close to the lateral pressure reported for biological membranes (30 mN/m),[44] indicating a high propensity of the probe for membrane insertion.[40] The same value was found for compound **14**, but a slightly lower one for probe **15.** Very recently, Salesse et

Table 2. Maximal Insertion Pressure Values (MIP), Synergy Factor (a), Initial Velocities of Surface Pressure Increase (V_i), and Log $P_{(oct/water)}$ for glycolipidic probes 13, 14, and 15

Probe	MIP (mN/m)	a	V_i (mN/m).min^{-1}	Log P
13	25.9	0.245	1.2	1.4
14	25.8	0.425	6.0	0.9
15	23.8	0.411	4.2	1.1

al.[45,46] introduced a new parameter to further analyze the plot of maximal surface pressure variation ($\Delta\pi$) versus initial surface pressure (π_i). This parameter corresponds to the synergy factor (a) calculated from the linear regression of $\Delta\pi$ as a function of π_i by adding 1 to the value of the slope. According to Salesse et al., a MIP with a positive synergy value ($a > 0$) corresponds to a favorable interaction between the molecules and the lipids. It reflects to a synergistic effect between the lipid compaction and the insertion ability.

The higher factor of synergy (a) for probes **14** and **15** can be correlated to their faster penetration kinetics (Table 2) that reveals an efficient membrane insertion activity for both probes. The factor of synergy for the disaccharidic probe **13** is lower. In this case, the presence of two saccharidic moieties insufficiently enhances the hydrophilic character and does not give an optimal amphipathic balance for a synergistic interaction with the monolayer. However, the lower MIP value obtained for probe **15** seems to indicate that the presence of a ramified trisaccharide with a wedge-like overall shape appears slightly less favorable for penetration than probe **14** with a linear trisaccharide. This result could be ascribed to the steric hindrance of the polar headgroup of the probe **15** when it inserts between the PC head groups of the monolayer. For probes **13**−**15**, the isotherms representing the surface pressure of the monolayer were studied as a function of the molecular area. A representative example is given for probe **14** in Figure 4. After penetration, the isotherm shifted toward

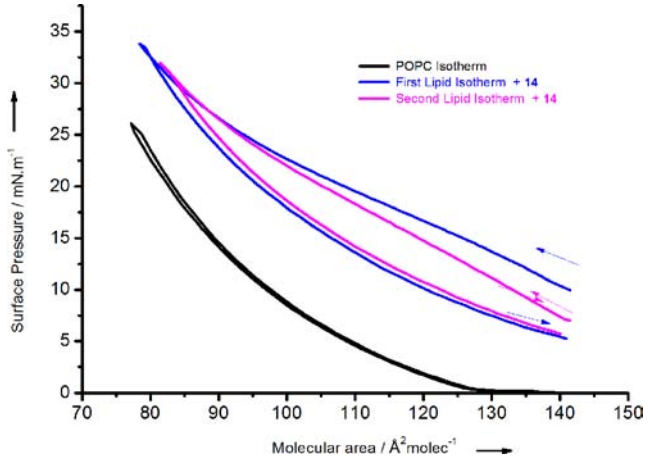

Figure 4. Surface pressure versus molecular area isotherm diagrams recorded during the interfacial film compression−decompression of a POPC monolayer before and after penetration of probe **14**.

larger molecular areas compared to pure POPC due to the presence of the probe embedded in the monolayer. This shift was observed all along the isotherm curve indicating that after insertion the probe remained in the monolayer even at high surface pressures. As shown in Figure 4, the compression/expansion cycle of the monolayer did not reduce the shift and the second cycle led to a very similar isotherm, reflecting the stability

dx.doi.org/10.1021/bc500047r | Bioconjugate Chem. 2014, 25, 773−787

A

Probe	Loading conditions ([DMSO])	Percentage laser transmission	PMT gain	Staining
Di-4-ANEPPS	5 μM / 5 min (1/1000)	20 %	(730-830)	Plasma membrane
Di-8-ANEPPS	5 μM / 10 min (1/1000)	20 %	(730-830)	Plasma membrane
13	5 μM / 5 min (1/1000)	20 %	(700-850)	Plasma membrane
14	5 μM / 5 min (1/1000)	20 %	(730-830)	Plasma membrane
15	5 μM / 5 min (1/1000)	20 %	(780-800)	Plasma membrane
16	5 μM / 35 min (1/1000)	70 %	(700-850)	No specific staining
17	5 μM / 5 min (1/1000)	20 %	(700-850)	Endoplasmic reticulum
18	10 μM / 30 min (1/500)	80 %	(720-850)	No staining
19	10 μM / 30 min (1/500)	20 %	(730-850)	Plasma membrane

B

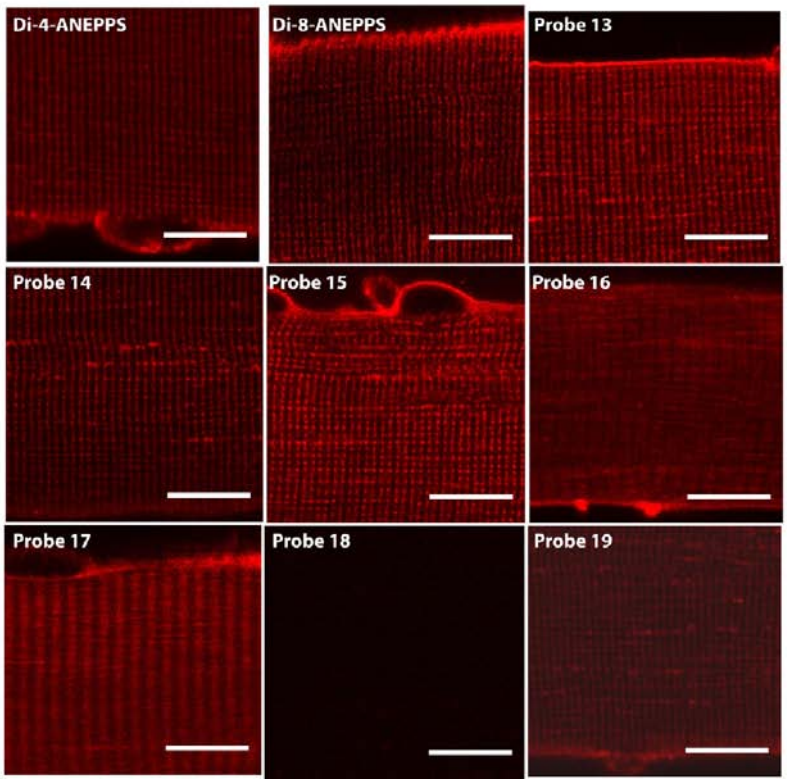

Figure 5. Comparison of loading, imaging conditions and targeting of the glycoconjugates with two classical membrane probes: Di-4- and Di-8-ANEPPS. (A) Experiments were repeated 2−6 times for each probe, with similar results. For all images: excitation wavelength 488 nm, detection window >650 nm. (B) Confocal images (*xy*) of skeletal muscle fibers loaded with the different glycoconjugates. Scale bar = 10 μm.

of the lipid−probe interaction, as reported for other molecules.[43,47] The same observations were made for the probes **13** and **15** (data not shown). These results confirmed a stable incorporation of the probes into the POPC monolayer.

The morphology of the POPC monolayer at the air/water interface was observed by Brewster angle microscopy (BAM)[48,49] before and after probe insertion. BAM images were taken at an initial surface pressure of 5 mN/m (π_i) and when the surface pressure reached a plateau π_{max} (see Supporting Information). As shown in Figure S1, the POPC monolayer was homogeneous before injection with a typical morphology of monolayers in fluid phase (Liquid Expanded phase). Addition of probe **14** in the subphase underneath the POPC monolayer did not induce structural modifications. All along the penetration of probe **14** within the monolayer, the morphology did not change (see SI, Figure S1). The same observations on POPC were made for the probes **13** and **15** indicating that these three probes induced no specific phospholipid reorganization, and hence membrane perturbation.

In order to confirm these results, probe **14** was injected into a subphase underneath a 1,2-dipalmitoylphosphatidylcholine (DPPC) monolayer initially compressed at 5 mN/m. DPPC was chosen because its isotherm phase transition plateau is more sensitive to morphology changes. BAM images (Figure S2) showed the liquid expanded to liquid condensed phase transition of the DPPC monolayer, with the presence of characteristic condensed domains (bright domain) surrounded by a fluid phase (dark background). After probe insertion, the condensed

dx.doi.org/10.1021/bc500047r | *Bioconjugate Chem.* 2014, 25, 773−787

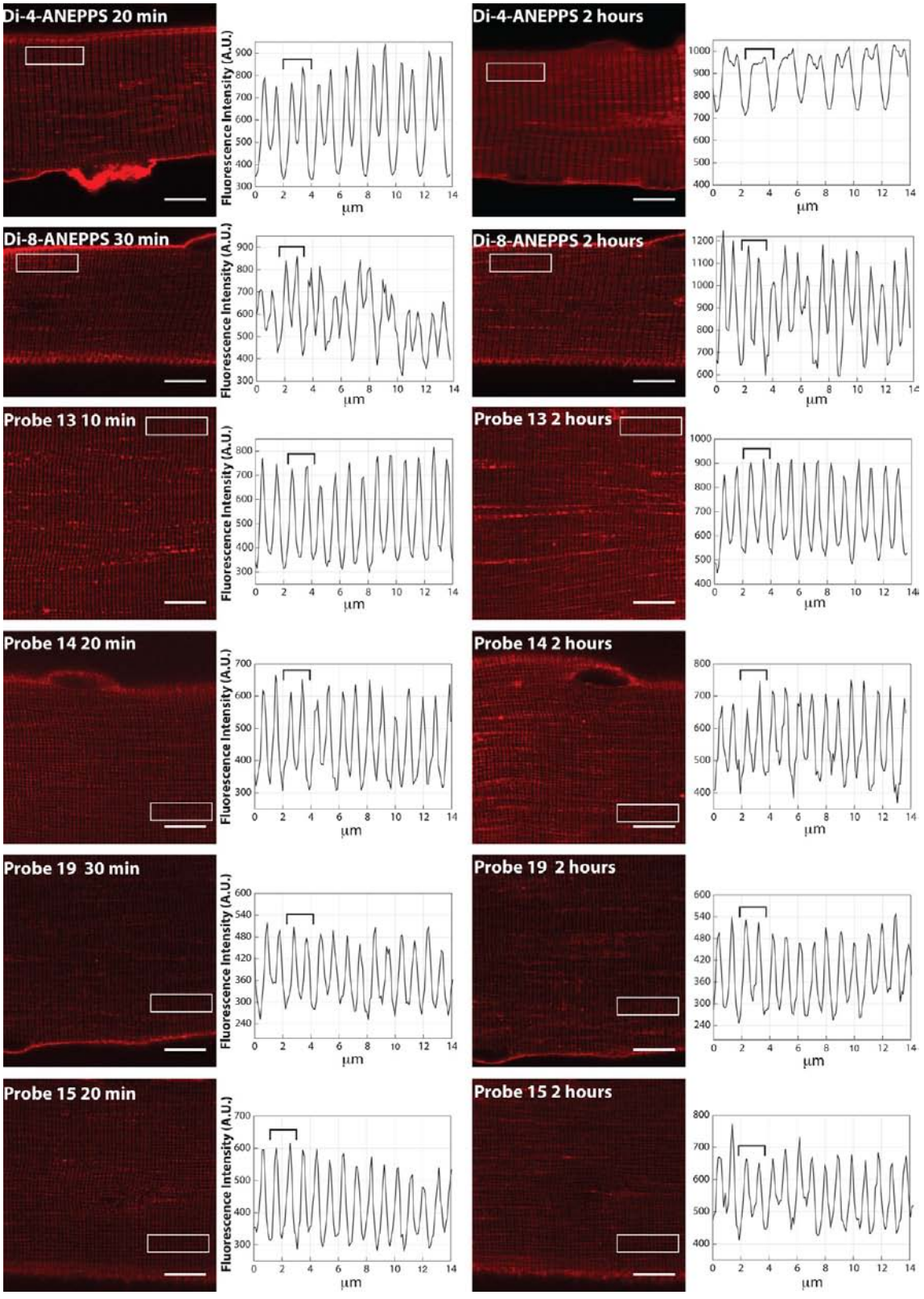

Figure 6. Targeting of ANEPPS and glycoprobes shortly after (left) and 2 h after (right) loading: Pictures are confocal images (*xy*) of fluorescence of skeletal muscle fibers loaded with the indicated probe. White bar = 10 μm. Graphs show the fluorescence intensity profile measured within the region of interest defined by the white box in the confocal image. Values are without brightness correction. Experiments were repeated on 3−6 cells for each probe, with similar results.

domains grew at 16.5 mN/m ($\Delta\pi_{max}$) surface pressure due to the surface pressure increase, but the lateral phospholipid organization remained unchanged. All these results indicate that probes **13**, **14**, and **15** exhibit high membrane penetration ability with stable interactions without generating lipid reorganization.

dx.doi.org/10.1021/bc500047r | *Bioconjugate Chem.* 2014, 25, 773−787

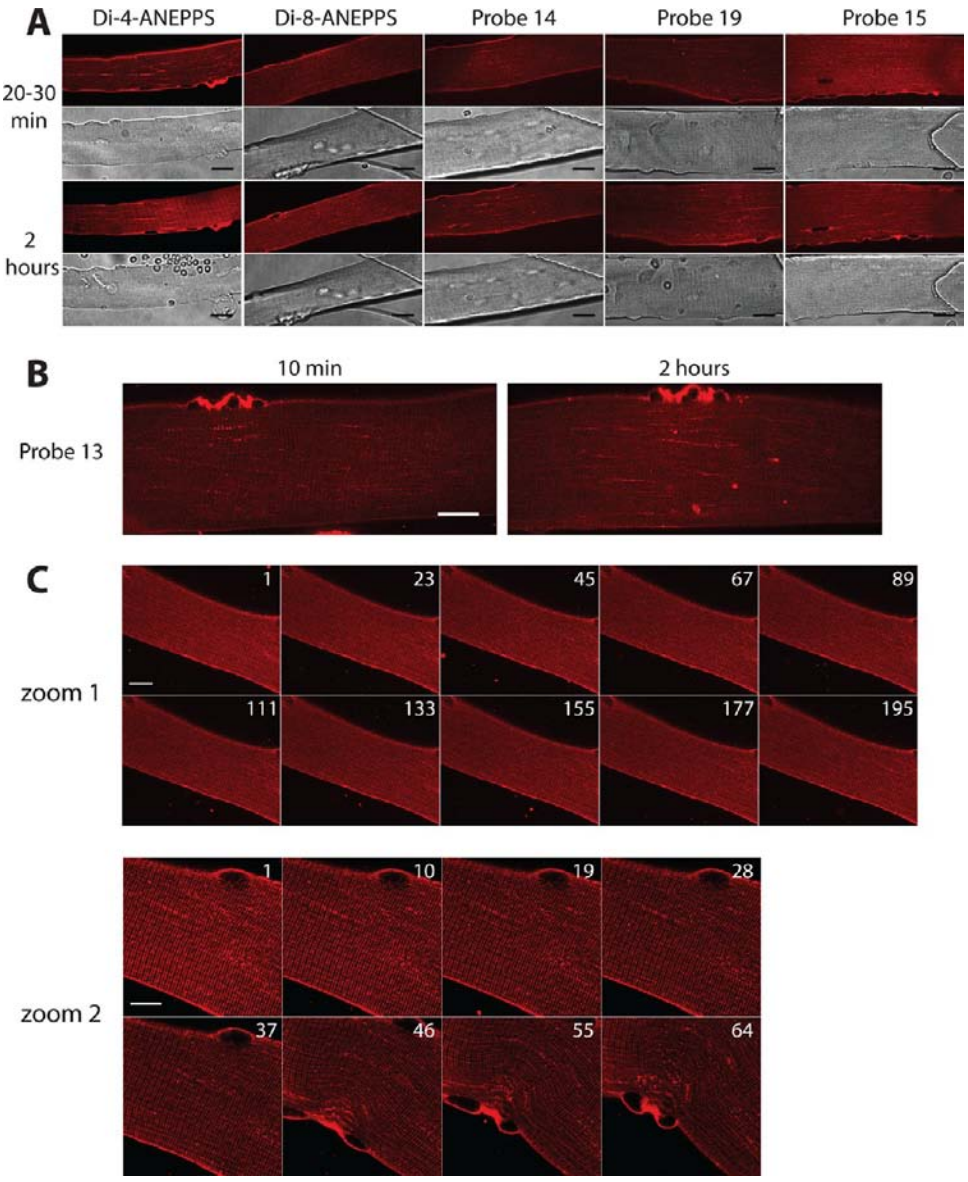

Figure 7. (A) Confocal images (*xy*) of fluorescence and transmitted images of skeletal muscle fibers loaded with Di-4-ANEPPS, Di-8-ANEPPS, probe **14**, probe **19**, and probe **15** shortly after and 2 h after loading. Black bar = 20 μm. Experiments were repeated on 3−6 cells for each probe, with similar results. (B) Confocal image (*xy*) of fluorescence of a skeletal muscle fiber loaded with probe **13** just after or 2 h after loading. White bar = 20 μm. (C) Confocal images (*xy*) of a skeletal muscle fiber loaded with probe **13** and repeatedly imaged with a zoom of 1 (195 times) or a zoom of 2 (64 times). Excitation wavelength was 488 nm; laser transmission 20%. Cell damage is only observed with a zoom of 2 (higher laser intensity per surface area), after 46 scans. White bar = 15 μm at zoom 1, 10 μm at zoom 2.

From the monolayer study, these probes appeared to be the best candidates for membrane imaging.

Confocal Imaging of Isolated Mouse Skeletal Muscle Cells. We tested the membrane targeting of all the glycoprobes on isolated skeletal cells.[24] Skeletal muscle fibers have a complex plasma membrane system, with a surface membrane and invaginations called T-tubules. These T-tubules are organized in transversally aligned doublets, appearing as paired transversal lines in *xy* confocal fluorescence images when stained with membrane markers (Figure S3). Hence, any probe targeted to the plasma membrane in skeletal muscle fiber should reproduce this pattern.

Probes were diluted in DMSO at a final concentration of 5 mM. This stock solution was then diluted in Tyrode to a final concentration of 5−10 μM, so that the final dilution of DMSO was 1/1000 or 1/500. All the probes tested were soluble under these conditions. Fibers were incubated with the different probes for 5−30 min (see Figure 5). Two classic membrane probes, Di-8-ANEPPS and Di-4-ANEPPS, handled in the same way, were used as reference. Similar recording conditions (laser intensity and PMT gain) were used to allow comparison between the different probes. Probe **18** was unable to stain the cell (Figure S4) while probe **16** gave an unspecific staining. Thus, both probes were not further investigated. Fibers loaded with probe **17** exhibited a transversal single line pattern (Figure 5), which does not correspond to specific plasma membrane staining. Co-staining of the cell with probe **17** and the dye ER Tracker Green showed that the probe **17** actually stained the sarcoplasmic reticulum (endoplasmic reticulum of skeletal muscle cells, Figure S5). Hence this probe was also discarded for the remainder of the study. All the remaining probes **13**, **14**, **15**, and **19**, as well as the

dx.doi.org/10.1021/bc500047r | *Bioconjugate Chem.* 2014, 25, 773−787

two reference probes, Di-4-ANEPPS and Di-8-ANEPPS, exhibited specific membrane staining.

Specificity and long-term retention of the probe in the plasma membrane was further tested. Figure 6 shows the targeting of different probes shortly after and 2 h after loading. The two reference probes, Di-4-ANEPPS and Di-8-ANEPPS, gave a relatively specific membrane staining just after loading. However, only Di-8-ANEPPS still showed specific staining after 2 h, whereas Di-4-ANEPPS appeared distributed inside the cytoplasm. Probes **13**, **14**, and **15** exhibited specific membrane staining and good retention of the signal after 2 h. The membrane staining was shown to be even sharper than the one obtained with the ANEPPS dyes. This can be seen on the line profile of the staining which shows sharper peaks of fluorescence intensity, corresponding to the T-tubule doublet for the glycoprobes **13**, **14**, and **15** than for the ANEPPS dyes (Figure 6). The fluorescence intensity of the glycoprobes was similar to the one obtained with the ANEPPS dyes. Despite the higher loading concentration and longer incubation time, probe **19** gave a dim (maximum = 540 AU) although specific staining.

Skeletal muscle fibers undergo permanent contraction and disruption of the T-tubule system (visualized as disruption of the alignment of the doublets under confocal microscopy) when damaged. Figure 7A and B show that cells loaded with either the ANEPPS dyes or the glycoprobes do not exhibit signs of alteration even after 2 h of staining. This result suggests that these membrane probes do not induce cytotoxicity under our experimental conditions. Figure 7C illustrates the lack of phototoxicity of the glycoprobes during the time course of our experiments using probe **13** as a model. The cell was repeatedly stimulated with a 488 nm laser wavelength with a zoom of 1× or 2×. 195 *xy* images at zoom 1× did not induce any visible damage, as shown by the absence of cell contraction and the preserved transversal alignment of the T-tubule system. Only at zoom 2×, providing a higher surface intensity of laser stimulation, and after 46 *xy* records did the cell start to exhibit signs of alteration (contraction). Overall those results show that the glycoprobes do not induce any noticeable photosensitization in our cell model under our experimental conditions.

Spectral properties can vary between *in vitro* and *in vivo* measurements. Hence we measured the emission spectrum of probe **13** loaded into skeletal muscle cells. The probe was excited at 488 nm and emission was recorded between 550 and 720 nm. Figure 8 shows that the probe exhibits a wide emission spectrum with a maximal intensity found at 643 nm. This corresponds to a 50 nm blue shift of the emission maximum compared to the spectra in pure water. Experiments were repeated on 3 cells, with comparable results. Similar fluorescence spectra were obtained with excitation at 514 nm (n = 3) and 561 nm (n = 3, results not shown). This emission corresponds more closely to that observed in octanol for similar fluorophores[26] suggesting that the probe is inserted in an apolar environment.

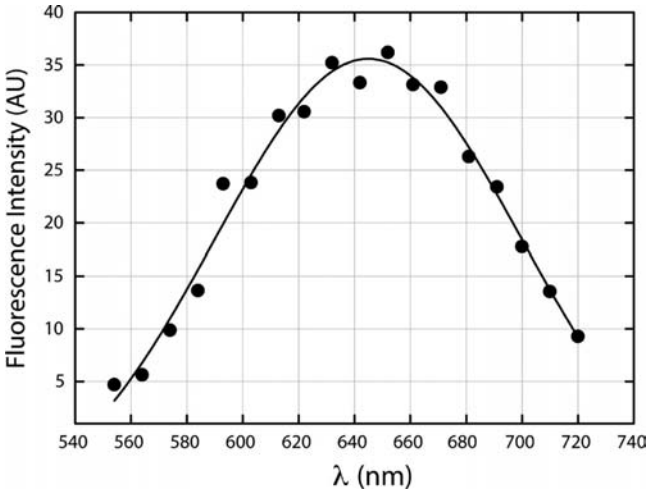

Figure 8. Spectral properties of probe **13**. The skeletal muscle fiber was excited at 488 nm and the emission was collected between 549 and 725 nm, with 9 nm incremental steps. Gaussian fit gives maximal intensity at 643 nm. Experiments were repeated on 3 cells, with similar results.

■ CONCLUSIONS

A series of new fluorescent membrane imaging glycoprobes were synthesized by careful tuning of the Cu(I) Huisgen cycloaddition reaction conditions on regioselectively functionalized azido-deoxysugars. Based on several carbohydrate scaffolds but using the same chromophore, they provided different structures showing a very large Stokes shift, with a maximum in absorption close to 505 nm and a maximum emission wavelength close to 690 nm. This large Stokes shift, the width of the absorption and emission bands with little overlap, as well as the high brightness values (1200−5000 L.mol^{-1}.cm^{-1}) make them attractive dyes from an optical point of view. The insertion properties of the different probes were first studied on a model system by using the Langmuir monolayer balance technique. The data collected showed diverse behavior for the different probes due to the varying overall structure of the molecules. The compounds consisting of one fluorophore attached, a linear disaccharidic (probe **13**), to a linear trisaccharidic(probe **14**) or a branched trisaccharidic (probe **15**) polar head, were found to insert faster and more efficiently than variants with either a larger chromophore or sugar content. Interestingly, BAM experiments showed that the insertion did not induce perturbation of the monolayer morphology anticipating a low biological toxicity. These results fit well the subsequent biological results, confirming this membrane monolayer technique as a good predicting tool for analyzing the biological behavior of new membrane probes. Biological experiments performed on muscle cells showed a completely different localization for the more lipophilic probes (**16**−**17**) or even no staining for the too hydrophilic probe **18**. Using the fact that muscle cells undergo contraction when damaged, probes **13**−**15** proved to be the most efficient membrane markers, for which neither obvious cytotoxicity nor phototoxicity were observed under our experimental conditions. When compared to di-4- or di-8-ANEPPS, commonly used dyes for membrane imaging, probes **13**−**15** showed similar fluorescence intensities but with a sharper pattern. All the above optical, physical, and biological properties establish probes **13**, **14**, and **15** as useful optical tools for membrane imaging experiments. Now synthesized and selected from a pool of potential probe candidates by both biophysical and biological experiments, these three probes (**13**−**15**) are currently being investigated for their nonlinear imaging properties. The dipolar fluorophore composing these probes is particularly attractive for that purpose, as it has been shown to display interesting second-order[50] and third-order nonlinear[27] optical properties. Studies have started on combined Two Photon Excited Fluorescence and Second Harmonic Imaging microscopy, notably to evaluate the performance of the dyes on reporting membrane potential change.

MATERIALS AND METHODS

Solvents were of HPLC or reagent quality and purchased commercially. Starting materials were purchased commercially and used without further purification. Compounds were characterized by using ^{1}H and ^{13}C NMR spectroscopy. The spectra were recorded on a Bruker AC 200 operating at 200.13 MHz for ^{1}H and 50.32 MHz for ^{13}C and on a Bruker Advance operating at 500.10 MHz for ^{1}H and 125.75 MHz for ^{13}C. Chemical shifts are reported as δ values (ppm) with reference to the residual solvent peaks. For proton, data are reported as follows: chemical shift, multiplicity (s = singlet, d = doublet, t = triplet, q = quartet, m = multiplet, b = broad), coupling constants in Hz. UV/vis absorption measurements were recorded on a JASCO V550 spectrometer. Fluorescence spectra were measured using a Horiba-Jobin Yvon Fluorolog-3 spectrofluorimeter, equipped with a red-sensitive Hamamatsu R928 photomuliplier tube. Spectra were reference corrected for both the excitation source light intensity variation (lamp and grating) and the emission spectral response (detector and grating). All solvents were of spectrophotometric grade. Erythrosin B was purchased from Acros. All air- or moisture-sensitive reactions were carried out in flame-dried glassware under Ar atmosphere. DMF was freshly distilled over CaH_2. Thin-layer chromatography (tlc) was performed with Merck 60F254 precoated silica gel plates. Column chromatography was carried out using Merck silica gel 60 (70−230 mesh). Azido-carbohydrates **6b**, **7b**, **8b**, **9b** were prepared as previously reported.[23]

Caution! Hydrazoic acid is toxic and shock sensitive when undiluted. Handle only diluted solutions, using an appropriate shielding and appropriate safety precautions.

***N,N*-Bis(2-(prop-2-ynyloxy)ethyl)aniline (2b).** 2,2′-(Phenylazanediyl)diethanol (2 g, 11.0 mmol) in dry DMF was cooled to 0 °C under argon. NaH 60% in oil (864 mg, 22.6 mmol, 2.1 equiv) was slowly added and the mixture was stirred for 1 h. A solution of propargylbromide (80% in toluene) (3.6 mL, 33.4 mmol, 3.1 equiv) was slowly added to the mixture at 0 °C and the solution was stirred at room temperature overnight. The brown solution was quenched by addition of water, the aqueous layer was extracted three times with Et_2O and the combined organic phases were washed three times with water, once with brine, dried over sodium sulfate, filtered, and concentrated under reduced pressure. The crude product was purified by column chromatography (dichloromethane/pentane: 1/1) to obtain a light brown oil (2 g, 72%). ^{1}H NMR (200 MHz, $CDCl_3$, TMS): δ = 7.82 (dd, ^{3}J(H,H) = 6 Hz, ^{3}J(H,H) = 8 Hz, 2H, Ar−H), 7.32 (m, 3H, Ar−H), 4.75 (d, ^{3}J(H,H) = 2 Hz, 4H, CH_2), 4.25 (m, 8H, CH_2), 3.04 ppm (t, ^{3}J(H,H) = 2 Hz, 2H, CH); ^{13}C NMR (50 MHz, $CDCl_3$): 148, 129, 116, 112, 80, 75, 67, 58, 51 ppm; IR (KBr): ν = 3298, 2116, 648 cm^{-1}; HRMS (TOF): m/z calcd for $C_{16}H_{20}NO_2$: 258.1489; found 258.1489; elemental analysis calcd (%) for $C_{16}H_{19}NO_2$: C 74.68, H 7.44, N 5.44; found: C 81.02, H 7.55, N 5.44.

***N*-Ethyl-*N*-(2-(prop-2-ynyloxy)ethyl)aniline (2a).** 2-(*N*-ethylanilino)ethanol (2 g, 12.1 mmol) in dry DMF was cooled to 0 °C under argon. NaH 60% in oil (484 mg, 12.1 mmol) was slowly added and the mixture was stirred during 1 h. A solution of propargylbromide (80% in toluene) (2.6 mL, 23.6 mmol) was slowly added to the mixture at 0 °C and the solution was stirred at room temperature overnight. The brown solution was quenched by addition of water, the aqueous layer was extracted three times with Et_2O, and the combined organic phases were washed three times with water, once with brine, dried over sodium sulfate, filtered, and concentrated under reduced pressure. The crude product was purified by column chromatography (dichloromethane/pentane: 1/1) to obtain a light brown oil. Yield: 1.89 g (77%). ^{1}H NMR (200 MHz, $CDCl_3$): δ = 7.83 (dd, ^{3}J(H,H) = 6 Hz, ^{3}J(H,H) = 8 Hz, 2H, Ar−H), 7.31 (m, 3H, Ar−H), 4.79 (d, ^{3}J(H,H) = 2 Hz, 2H, CH_2), 4.31 (t, ^{3}J(H,H) = 6 Hz, 2H, CH_2), 4.15 (t, ^{3}J(H,H) = 6 Hz, 2H, CH_2), 4.03 (q, ^{3}J(H,H) = 6 Hz, 2H, CH_2), 3.05 (t, ^{4}J(H,H) = 2 Hz, 1H, CCH); 1.79 ppm (t, ^{3}J(H,H) = 6 Hz, 3H, CH_3); ^{13}C NMR (50 MHz, $CDCl_3$): δ = 148, 129, 116, 112, 80, 75, 68, 58, 50, 45, 12 ppm; IR (KBr): ν = 3298, 2116, 648 cm^{-1}; HRMS (TOF): m/z calcd for $C_{13}H_{17}NO$: 204.1388; found 204.1384; elemental analysis calcd for $C_{13}H_{17}NO$: C 76.81, H 8.43, N 6.89; found: C 77.37, H 8.46, N 6.90.

4-(Bis(2-(prop-2-ynyloxy)ethyl)amino)benzaldehyde (3b). The solution of aniline derivative **2b** (5.6 g, 22 mmol, 1 equiv) in dry DMF (17 mL) was cooled to 0 °C under argon. $POCl_3$ (4.1 mL, 44 mmol) was slowly added. The mixture was stirred for 12 h at 40 °C. After cooling to room temperature, the green solution was poured into ice water and carefully neutralized with solid K_2CO_3. The aqueous layer was extracted three times with CH_2Cl_2 and the combined organic phases were washed three times with water, once with brine, dried over sodium sulfate, filtered, and concentrated under reduced pressure to afford light brown solid **3b** (5.78 g, 92%). mp 74−75 °C; ^{1}H NMR (200 MHz, $CDCl_3$): δ = 9.61 (s, 1H, CHO), 7.61 (d, ^{3}J(H,H) = 10 Hz, 2H, Ar−H), 6.69 (d, ^{3}J(H,H) = 10 Hz, 2H, Ar−H), 4.06 (d, ^{4}J(H,H) = 2 Hz, 4H, CH_2), 3.63 (m, 8H, CH_2), 2.41 ppm (t, ^{4}J(H,H) = 2 Hz, 2H, CCH); ^{13}C NMR (50 MHz, $CDCl_3$): δ = 189, 152, 131, 125, 111, 79, 78, 67, 58, 51 ppm; IR (KBr): ν = 3246, 2864, 2109, 1689, 681 cm^{-1}; HRMS (TOF): m/z calcd for $C_{17}H_{20}NO_3$: 286.1443; found 286.1433; elemental analysis calcd (%) for $C_{17}H_{19}NO_3$: C 71.56, H 6.71, N 4.91; found: C 71.43, H 6.66, N 4.92.

4-(Ethyl(2-(prop-2-ynyloxy)ethyl)amino)-benzaldehyde (3a). The solution of aniline derivative **2a** (4.3 g, 21 mmol, 1 equiv) in dry DMF (16.5 mL) was cooled to 0 °C under argon . $POCl_3$ (3.9 mL, 42 mmol) was slowly added. The mixture was stirred for 12 h at 40 °C. After cooling to room temperature, the green solution was poured into ice water and carefully neutralized with solid K_2CO_3. The aqueous layer was extracted three times with CH_2Cl_2 and the combined organic phases were washed three times with water, once with brine, dried over sodium sulfate, filtered, and concentrated under reduced pressure to afford dark brown solid **3a** (4.76 g, 98%). ^{1}H NMR (200 MHz, $CDCl_3$): δ = 9.72 (s, 1H, CHO), 7.71 (d, ^{3}J(H,H) = 8 Hz, 2H, Ar−H), 6.71 (d, ^{3}J(H,H) = 8 Hz, 2H, Ar−H), 4.16 (d, ^{4}J(H,H) = 2 Hz, 2H, CH_2), 3.72 (t, ^{3}J(H,H) = 6 Hz, 2H, CH_2), 3.61 (t, ^{3}J(H,H) = 6 Hz, 2H, CH_2), 3.51 (q, ^{3}J(H,H) = 6 Hz, 2H, CH_2), 2.43 (t, ^{4}J(H,H) = 2 Hz, 1H, CCH), 1.21 ppm (t, ^{3}J(H,H) = 6 Hz, 3H, CH_3); ^{13}C NMR (50 MHz, $CDCl_3$): δ = 189, 152, 132, 125, 111, 79, 74, 67, 58, 49, 45, 12; IR (KBr): ν = 3284, 2869, 2113, 1666, 710 cm^{-1}; HRMS (TOF): m/z calcd for $C_{14}H_{17}NO_2Na$: 254.1157; found 254.1166; elemental analysis calcd (%) for $C_{14}H_{17}NO_2$: C 72.70, H 7.41, N 6.06; found: C 73.56, H 7.42, N 6.06.

(*E*)-2-(3-(4-(Bis(2-(prop-2-ynyloxy)ethyl)amino)styryl)-5,5-dimethylcyclohex-2-enylidene)malononitrile (5b). To a solution of **3b** (5.3 g, 18 mmol) and 2-(3,5,5-trimethylcyclohex-2-enylidene)malononitrile (3.6 g, 20 mmol) in dry acetonitrile (100 mL) under argon was added a catalytic amount of piperidine (20 μL, 0.2 mmol). The mixture was stirred at room temperature for 12 h. The red solution was concentrated

dx.doi.org/10.1021/bc500047r | *Bioconjugate Chem.* 2014, 25, 773−787

under reduced pressure and the crude product purified by column chromatography (dichloromethane/pentane: 2/1) to obtain a dark red solid. Yield: 7.9 g (87%). mp 102−103 °C; ^{1}H NMR (200 MHz, $CDCl_3$): δ = 7.38 (d, ^3J(H,H) = 10 Hz, 2H, Ar−H), 7.00 (d, ^3J(H,H) = 16 Hz, 1H, CH), 6.73 (m, 4H, Ar−H + CH), 4.15 (d, ^4J(H,H) = 2 Hz, 4H, CH_2), 3.68 (m, 8H, CCH + CH_2), 2.55 (s, 2H, CH_2), 2.43 (s, 4H, CH_2), 1.05 ppm (s, 6H, CH_3); ^{13}C NMR (50 MHz, $CDCl_3$): δ = 169, 155, 149, 138, 129, 125, 124, 122, 114, 113, 112, 80, 75, 67, 59, 51, 43, 39, 32, 28 ppm; IR (KBr): ν = 3284, 3049, 2866, 2208, 1550, 1508, 1182, 1106 cm^{-1}; HRMS (TOF): m/z calcd for $C_{29}H_{32}N_3O_2$: 454.2495; found 454.2506; elemental analysis calcd (%) for $C_{29}H_{31}N_3O_2$: C 76.79, H 6.89, N 9.26; found: C 76.64, H 7.06, N 9.18.

(*E*)-2-(3-(4-(Ethyl(2-(prop-2-ynyloxy)ethyl)amino)-styryl)-5,5-dimethylcyclohex-2-enylidene)malononitrile (5a). To a solution of **3a** (4.5 g, 19 mmol) and 2-(3,5,5-trimethylcyclohex-2-enylidene)malononitrile (3.6 g, 20 mmol) in dry acetonitrile (100 mL) under argon was added a catalytic amount of piperidine (20 μL, 0.2 mmol). The mixture was stirred at room temperature for 12 h. The red solution was concentrated under reduced pressure and the crude product purified by column chromatography (dichloromethane/pentane: 2/1) to obtain a dark red solid. Yield: 7.4 g (92%). mp 116−117 °C; ^{1}H NMR (200 MHz, CD_2Cl_2): δ = 7.39 (d, ^3J(H,H) = 10 Hz, 2H, Ar−H), 7.03 (d, ^3J(H,H) = 15 Hz, 1H, CH), 6.82 (d, ^3J(H,H) = 15 Hz, 1H, CH), 6.70 (m, 3H, Ar−H + CH), 4.16 (s, 2H, CH_2), 3.69 (t, ^3J(H,H) = 5 Hz, 2H, CH_2), 3.56 (t, ^3J(H,H) = 5 Hz, 2H, CH_2), 3.46 (q, ^3J(H,H) = 5 Hz, 2H, CH_2), 2.53 (s, 2H, CH_2), 2.48 (s, 1H, CH), 2.44 (s, 2H CH_2), 1.18 (t, ^3J(H,H) = 5 Hz, 3H, CH_3), 1.04 ppm (s, 6H, CH_3); ^{13}C NMR (50 MHz, CD_2Cl_2): δ = 170, 156, 149, 138, 130, 125, 124, 122, 115, 114, 112, 80, 76, 75, 68, 59, 50, 46, 43, 40, 32, 28, 12 ppm; IR (KBr): ν = 3268, 2951, 2872, 2215, 1596, 1546, 1506, 1178 cm^{-1}; HRMS (TOF): m/z calcd for $C_{26}H_{30}N_3O$: 400.2389; found 400.2393; elemental analysis (%) calcd for $C_{26}H_{29}N_3O$: C 78.16, H 7.32, N 10.52; found: C 78.28, H 7.44, N 10.56.

6-*O*-Benzoyl-α-D-glucopyranosyl-(1→3)-β-D-fructofuranoside 6-*O*-benzoyl-α-D-glucopyranoside (di-6,6″-*O*-benzoyl melezitose) 11. A solution of melezitose (2.08 g, 4.1 mmol) in DMF (80 mL) was first dried by concentrating under vacuum to a 60 mL volume. PPh_3 (4.2 g, 4 equiv) and benzoic acid (1.9 g, 4 equiv) were added and the obtained solution was then cooled to 0 °C and placed under N_2. DIAD (3.2 mL, 4 equiv) was then added and the reaction was left to warm up to room temperature over 1 h, then it was further stirred for 24 h. The obtained solution was concentrated and directly subjected to silica gel chromatography using a dichloromethane/acetone/methanol/water gradient (three different ratios were employed: 78/10/10/2, 67/15/15/3) to give tribenzoyl **10** (0.8 g, 24%) and dibenzoyl compounds **11** (1 g, 35%).$[\alpha]_D$ = +79 (c = 0.6 in methanol). ^{1}H NMR (500 MHz, [D_4]methanol): δ = 8.22−8.20 (m, 4H), 7.76−7.74 (m, 2H), 7.65−7.61 (m, 4H), 5.69 (d, ^3J(H,H) = 4.0 Hz, 1H), 5.39 (d, ^3J(H,H) = 4.0 Hz, 1H), 4.84−4.78 (m, 2H), 4.75−4.69 (m, 2H), 4.50−4.48 (m, 2H), 4.45−4.40 (m, 2H), 4.02−3.80 (m, 7H), 3.80−3.65 ppm (m, 4H); ^{13}C NMR (125 MHz, [D_4]methanol): δ = 168.2, 168.1, 131.2, 131.2, 130.6, 130.6, 129.5, 129.5, 129.4, 75.2, 74.9, 74.7, 73.5, 73.5, 72.9, 71.8, 71.7, 71.7, 71.6, 71.6, 65.2, 65.0, 64.4, 63.8 ppm. HRMS (EI+): m/z calculated for $C_{32}H_{40}O_{18}$ + Na^+: 735.2112; found: 735.2107.

6-*O*-Benzoyl-α-D-glucopyranosyl-(1→3)-6-*O*-azido-β-D-fructofuranoside 6-*O*-benzoyl-α-D-glucopyranoside 12a. To a solution of dibenzoyl melezitose **11** (500 mg, 0.7 mmol) and PPh_3 (0.9 g, 5 equiv) in DMF (10 mL) at 0 °C under N_2 was added a 5% HN_3 solution in toluene (3.8 mL), prepared under N_2. DIAD (0.7 mL, 5 equiv) was then added slowly and the reaction was left to warm up to room temperature over 1 h, then it was further stirred for 24 h. Water (50 mL) was then added and the solution was neutralized using a 28% ammonia solution. The obtained solution was evaporated under vacuum and the residue was subjected to silica gel chromatography using a dichloromethane/acetone/methanol/water mixture (78/10/10/2) to give monoazide **12a** (180 mg, 35%). R_f = 0.27 (dichloromethane/acetone/methanol/water: 78/10/10/2); $[\alpha]_D$ = +80 (c = 0.6 in methanol); ^{1}H NMR (300 MHz, [D_4]methanol): δ = 8.10−8.07 (m, 4H), 7.66−7.61 (m, 2H), 7.55−7.48 (m, 4H), 5.53 (d, ^3J(H,H) = 3.9 Hz, 1H), 5.39 (d, ^3J(H,H) = 3.9 Hz, 1H), 4.80−4.48 (m, 4H), 4.35−4.24 (m, 4H), 4.95−3.35 (m, 9H), 3.15 ppm (dd, ^3J(H,H) = 12.8, 3.0 Hz, 1H); ^{13}C NMR (125 MHz, [D_4]methanol): δ = 168.2, 168.1, 131.2, 131.2, 130.6, 130.6, 129.5, 129.5, 129.4, 75.2, 74.9, 74.7, 73.5, 73.5, 72.9, 72.8, 71.8, 71.7, 71.7, 71.6, 71.6, 65.2, 65.0, 64.4 ppm. HRMS (EI+): m/z calculated for $C_{32}H_{39}N_3O_{17}$: 737.6620; found: 737.6611.

α-D-Glucopyranosyl-(1→3)-6-*O*-azido-β-D-fructofuranoside α-D-glucopyranoside 12b. To a solution of **12a** (100 mg, 0.14 mmol) in methanol (2 mL) was added a molar solution of potassium hydroxide (1 M in water, 300 μL, 4 equiv). After stirring 30 min the solution was concentrated under vacuum. The residue was purified by silica gel chromatography to afford **12b** (72 mg, 80%). $[\alpha]_D$ = +76 (c = 0.6 in methanol); ^{1}H NMR (300 MHz, D_2O): δ = 5.52−5.51 (d, ^3J(H,H) = 3.8 Hz, 1H), 5.28 (d, ^3J(H,H) = 3.8 Hz, 1H), 4.45−4.40 (m, 2H), 4.08 (m, 4H), 4.35−4.24 (m, 4H), 4.95−3.35 (m, 9H), 3.15 ppm (dd, ^3J(H,H) = 12.8, 3.0 Hz, 1H); ^{13}C NMR (125 MHz, [D_4]methanol): δ = 101.4, 93.6, 85.3, 83.8, 75.3, 73.6, 73.1, 72.0, 71.9, 71.8, 71.8, 65.3, 65.2, 64.6, 64.0 ppm. HRMS (EI+): m/z calculated for $C_{18}H_{31}N_3O_{15}$: 529.4498; found: 529.4485.

Synthesis and Characterization of Carbohydrate Based Probes. *Procedure A. Compound **13**.* A solution of β-D-fructofuranosyl 6-azido-6-deoxy-α-D-glucopyranoside (6-azido-6-deoxy-saccharose) **6b** (48 mg, 0.13 mmol), **5a** (40 mg, 0.1 mmol), and copper iodide (0.5 mg, 0.003 mmol) in methanol (2 mL) was heated at 65 °C for 14 h. The reaction mixture was then concentrated under vacuum and the residue was purified by column chromatography on silica gel eluting with dichloromethane/acetone/methanol/water (67:15:15:3) affording a dark red solid (50 mg, 65%). R_f = 0.25 (dichloromethane/acetone/methanol/water: 67/15/15/3); ^{1}H NMR (300 MHz, [D_4]methanol): δ = 7.90 (s, 1H), 7.46 (d, ^3J(H,H) = 8.8 Hz, 2H), 7.18 (d, ^3J(H,H) = 15.8 Hz, 1H), 6.90 (d, ^3J(H,H) = 15.8 Hz, 1H), 6.73 (d, ^3J(H,H) = 8.8 Hz, 3H), 5.34 (d, ^3J(H,H) = 3.8 Hz, 1H), 4.67−4.60 (m, 1H), 4.63 (s, 2H), 4.25−4.20 (m, 1 H), 4.05 (d, ^3J(H,H) = 7.9 Hz, 1H), 3.75−3.75 (m, 4H), 3.60−3.48 (m, 4H), 3.65−3.60 (m, 1 H), 3.02 (t, ^3J(H,H) = 9.1 Hz, 1H), 2.58 (s, 2H), 2.55 (s, 2H), 1.17 (t, ^3J(H,H) = 6.9 Hz, 3H), 1.08 ppm (s, 6H); ^{13}C NMR (50 MHz, [D_4]methanol): δ = 171.0, 158.0, 150.8, 140.2, 131.0, 125.0, 124.8, 121.7, 115.3, 114.6, 113.0, 105.3, 93.5, 83.6, 79.0, 74.3, 72.0, 69.3, 65.1, 63.9, 52.1, 50.8, 46.5, 43.9, 39.9, 32.8, 28.2, 12.6 ppm; IR (KBr): ν = 2216 (ν_{CN}), 3411 (ν_{OH}) cm^{-1}; HRMS (EI+): m/z calculated for $C_{38}H_{51}N_6O_{11}$: 767.3610; found: 767.3643.

*Example of Procedure B. Compound **14**.* A solution of α-D-galactopyranosyl-(1→6)-α-D-glucopyranosyl 6-azido-6-deoxy-β-D-fructofuranoside (6-azido-6-deoxyraffinose) **8b** (100 mg, 0.19 mmol), **5a** (65 mg, 0.16 mmol), and CuI·P(OEt)$_3$ (10 mg, 0.025

dx.doi.org/10.1021/bc500047r | *Bioconjugate Chem.* 2014, 25, 773−787

mmol) in methanol/chloroform (0.6 mL/0.3 mL) was heated at 100 °C in sealed tube for 3 h under microwave irradiations (performed on a Biotage Initiator system). The reaction mixture was then concentrated under vacuum and the residue was purified by column chromatography on silica gel using a dichloromethane/acetone/methanol/water mixture (67:15:15:3) to afford a dark red solid (80 mg, 54%). ^{1}H NMR (500 MHz, [D$_4$]methanol): δ = 8.02 (s, 1H), 7.45 (d, ^3J(H,H) = 8.8 Hz, 2H), 7.15 (d, ^3J(H,H) = 8.8 Hz, 1H), 6.88 (d, ^3J(H,H) = 8.8 Hz, 1H), 6.72 (d, ^3J(H,H) = 8.8 Hz, 2H), 6.69 (s, 1H), 5.36 (d, ^3J(H,H) = 3.8 Hz, 1H), 4.78−4.87 (m, 2H), 4.62 (s, 2H), 4.20−4.18 (m, 1H), 4.13−4.08 (m, 3H), 3.92 (dd, ^3J(H,H) = 11.5, 6.1 Hz, 1H), 3.77−3.73 (m, 3H), 3.72−3.68 (m, 5H), 3.64 (dd, ^3J(H,H) = 12.4, 6.3 Hz, 1H), 3.60−3.46 (m, 8H), 2.54 (s, 2H), 2.52 (s, 2H), 1.16 (t, ^3J(H,H) = 6.9 Hz, 3H), 1.06 ppm (s, 6H); ^{13}C NMR (125 MHz, [D$_4$]methanol): δ = 171.1, 158.2, 150.8, 140.3, 131.1, 126.4, 125.0, 124.9, 124.9, 121.7, 115.3, 112.9, 105.9, 101.0, 93.6, 81.5, 77.6, 75.2, 74.4, 73.6, 73.0, 72.4, 72.1, 71.2, 70.9, 70.2, 62.7, 65.0, 63.6, 62.7, 54.6, 50.9, 46.5, 44.0, 39.9, 32.8, 28.2, 12.6 ppm; IR (KBr): ν = 2216 (ν_{CN}), 3411 (ν_{OH}) cm^{-1}; HRMS (EI+): m/z calculated for $C_{44}H_{61}N_6O_{16}$: 929.4139; found: 929.4096.

Compound ***15***. Obtained according to procedure B from azide **12b** (40 mg, 75 μmol), alkyne **5a** (30 mg, 75 μmol), and a catalytic amount of CuI·P(OEt)$_3$. Purification by column chromatography on silica gel eluting with dichloromethane/acetone/methanol/water (67/15/15/3) gave a dark red solid (63 mg, 90%). R_f = 0.24 (dichloromethane/acetone/methanol/water: 67/15/15/3); ^{1}H NMR (500 MHz, [D$_4$]methanol): δ = 8.11 (s, 1H), 7.46 (d, ^3J(H,H) = 8.5 Hz, 2H), 7.17 (d, ^3J(H,H) = 15.5 Hz, 1H), 6.90 (d, ^3J(H,H) = 15.5 Hz, 1H), 6.72 (d, ^3J(H,H) = 8.5 Hz, 3H), 5.43 (d, ^3J(H,H) = 3.5 Hz, 2H), 5.11 (d, ^3J(H,H) = 3.5 Hz, 2H), 4.93−4.90 (t, ^3J(H,H) = 5.6 Hz, 1H), 4.75 (d, ^3J(H,H) = 9.7 Hz, 3H), 4.63 (s, 2H), 4.41 (t, ^3J(H,H) = 4.5 Hz, 1H), 4.16 (d, ^3J(H,H) = 4.5 Hz, 2H), 4.05 (brs, 1H), 4.00−3.95 (m, 4H), 3.78 (d, ^3J(H,H) = 8.4 Hz, 1H), 3.75−3.68 (m, 6H), 3.65−3.47 (m, 4H), 2.56 (s, 2H), 2.54 (s, 2H), 1.32 (t, ^3J(H,H) = 6.9 Hz, 3H), 1.16 ppm (s, 6H); ^{13}C NMR (125 MHz, [D$_4$]methanol): δ = 171.1, 158.2, 150.8, 140.3, 131.0, 124.9, 121.7, 115.3, 114.6, 112.9, 106.1, 102.0, 93.5, 85.6, 81.2, 76.6, 75.2, 75.0, 74.7, 74.5, 73.9, 73.7, 73.1, 72.2, 72.0, 69.2, 63.6, 62.9, 54.4, 50.9, 46.5, 43.9, 39.9, 32.8, 28.2, 12.5 ppm. IR (KBr): ν = 2216 (ν_{CN}), 3400 (ν_{OH}) cm^{-1}; HRMS (EI+): m/z calculated for $C_{44}H_{61}N_6O_{16}$: 929.4139; found: 929.4107.

Compound ***16***. Obtained according to procedure B from azide **7b** (30 mg, 76 μmol), alkyne **5a** (60 mg, 150 μmol) and a catalytic amount of CuI·P(OEt)$_3$. Purification by column chromatography on silica gel eluting with dichloromethane/acetone/methanol/water (67/15/15/3) afforded a dark red solid (62 mg, 68%). R_f = 0.23 (dichloromethane/acetone/methanol/water: 78/10/10/2); ^{1}H NMR (500 MHz, [D$_4$]-methanol/CDCl$_3$ = 50/50): δ = 7.72 (s, 2H), 7.31 (d, ^3J(H,H) = 8.7 Hz, 4H), 6.99 (d, ^3J(H,H) = 16.0 Hz, 2H), 6.71 (d, ^3J(H,H) = 16.0 Hz, 2H), 6.61−6.58 (m, 6H), 4.64 (d, ^3J(H,H) = 3.4 Hz, 2H), 4.46 (dd, ^3J(H,H) = 14.3, 7.15 Hz, 2H), 4.14 (t, ^3J(H,H) = 7.3 Hz, 2H), 3.69 (t, ^3J(H,H) = 9.2 Hz, 2H), 3.59 (t, ^3J(H,H) = 5.5 Hz, 4H), 3.46 (t, ^3J(H,H) = 5.1 Hz, 4H), 3.34 (q, ^3J(H,H) = 7.0 Hz, 4H), 2.99 (t, ^3J(H,H) = 9.4 Hz, 2H), 3.77−3.73 (m, 3H), 3.72−3.68 (m, 5H), 3.64 (dd, ^3J(H,H) = 12.4, 6.3 Hz, 1H), 2.44 (s, 2H), 2.38 (s, 2H), 1.06 (t, ^3J(H,H) = 6.8 Hz, 3H), 0.97 ppm (s, 12H); ^{13}C NMR (125 MHz, [D$_4$]methanol/CDCl$_3$ = 50/50): δ = 169.6, 156.2, 149.0, 138.6, 129.6, 125.5, 123.7, 124.9, 120.6, 114.0, 113.2, 111.7, 93.9, 74.1, 72.7, 71.2, 71.1, 69.9, 67.6, 63.9, 50.8, 45.3, 42.6, 38.7, 31.6, 27.3, 11.5 ppm; IR (KBr): ν = 2216 (ν_{CN}), 3418 (ν_{OH}) cm^{-1}; HRMS (EI+): m/z calculated for $C_{64}H_{80}N_{12}O_{11}$ [M+2H]$^{2+}$: 596.3029; found: 596.3014.

Compound ***17***. Obtained according to procedure B from azide **9b** (100 mg, 170 μmol), alkyne **5a** (215 mg, 538 μmol), and catalytic amount of CuI·P(OEt)$_3$. Purification by column chromatography on silica gel eluting with dichloromethane/acetone/methanol/water (67/15/15/3) gave a dark red solid (218 mg, 72%). R_f = 0.42 (dichloromethane/acetone/methanol/water: 78/10/10/2); ^{1}H NMR (300 MHz, [D$_4$]methanol/CDCl$_3$ = 50/50): δ = 7.47 (s, 1H), 7.45 (s, 1H), 7.44 (s, 1H), 7.03 (m, 3H), 6.66 (m, 3H), 6.50−6.26 (m, 10H), 4.96 (s, 1H), 4.70 (s, 1H), 4.20 (s, 4H), 4.08 (s, 1H), 4.02−3.94 (m,2H), 3.84−3.75 (m, 2H), 3.75−3.68 (m, 4H), 3.65−3.55 (m, 4H), 3.48−3.28 (m, 6H), 3.25−3.18 (m, 6H), 3.10−3.05 (m, 6H), 2.90−2.60 (m, 6H), 2.16 (s, 6H), 2.09 (s, 6H), 0.75 (t, J = 6.9 Hz, 9H), 0.67 ppm (s, 18H); ^{13}C NMR (125 MHz, [D$_4$]methanol): δ = 171.1, 158.2, 150.8, 140.3, 131.0, 124.9, 121.7, 115.3, 114.6, 112.9, 106.1, 102.0, 93.5, 85.6, 81.2, 76.6, 75.2, 75.0, 74.7, 74.5, 73.9, 73.7, 73.1, 72.2, 72.0, 69.2, 63.6, 62.9, 54.4, 50.9, 46.5, 43.9, 39.9, 32.8, 28.2, 12.5 ppm. HRMS (EI+): m/z calculated for $C_{96}H_{117}N_{18}O_{16}$: 1777.8889; found: 1777.8889.

Compound ***18***. Obtained according to procedure B from azide **6b** (25 mg, 68 μmol), alkyne **5b** (10 mg, 22 μmol), and a catalytic amount of CuI·P(OEt)$_3$. Purification by column chromatography on silica gel eluting with dichloromethane/acetone/methanol/water (67/15/15/3) afforded a dark red solid (10 mg, 38%). R_f = 0.7 (dichloromethane/acetone/methanol/water: 30/30/30/10); ^{1}H NMR (500 MHz, [D$_4$]-methanol): δ = 7.94 (s, 2H), 7.47 (d, ^3J(H,H) = 9.0 Hz, 2H), 7.18 (d, ^3J(H,H) = 15.9 Hz, 1H), 6.93 (d, ^3J(H,H) = 15.9 Hz, 1H), 6.76 (d, ^3J(H,H) = 15.9 Hz, 2H), 7.74 (s, 1H), 5.36 (d, ^3J(H,H) = 3.6 Hz, 2H), 4.70−4.58 (m, 4H), 4.60 (s, 4H), 4.28−4.25 (m, 2H), 4.07 (d, ^3J(H,H) = 8.2 Hz, 2H), 3.80−3.68 (m, 15H), 3.60−3.50 (m, 8H), 3.36 (dd, ^3J(H,H) = 12.0, 6.8 Hz, 2H), 3.33 (d, ^3J(H,H) = 3.6 Hz, 1H), 3.05 (t, ^3J(H,H) = 9.3 Hz, 2H), 2.59 (s, 2H), 2.56 (s, 2H), 1.09 ppm (s, 6H). ^{13}C NMR (125 MHz, [D$_4$]methanol): δ = 171.2, 158.1, 150.8, 145.7, 140.1, 131.1, 125.3, 121.9, 115.2, 114.5, 113.2, 105.3, 93.5, 83.7, 79.1, 79.0, 74.3, 72.1, 69.1, 65.1, 64.0, 63.9, 52.2, 52.0, 44.0, 40.0, 32.9, 28.2 ppm. IR (KBr): ν = 2216 (ν_{CN}), 3420 (ν_{OH}) cm^{-1}; HRMS (EI+): m/z calculated for $C_{53}H_{74}N_9O_{22}$: 1188.4943; found: 1188.4886.

Compound ***19***. Obtained according to procedure B from azide **8b** (105 mg, 200 μmol), alkyne **5b** (30 mg, 66 μmol), and a catalytic amount of CuI·P(OEt)$_3$. Purification by column chromatography on silica gel eluting with dichloromethane/acetone/methanol/water (30/30/30/10) gave a dark red solid (80 mg, 81%). R_f = 0.38 (dichloromethane/acetone/methanol/water: 30/30/30/10); ^{1}H NMR (500 MHz, [D$_4$]methanol): δ = 8.02 (s, 2H), 7.46 (d, ^3J(H,H) = 8.8 Hz, 2H), 7.18 (d, ^3J(H,H) = 8.7 Hz, 1H), 6.90 (d, ^3J(H,H) = 8.7 Hz, 1H), 6.74 (d, ^3J(H,H) = 5.8 Hz, 3H), 5.37 (d, ^3J(H,H) = 3.6 Hz, 2H), 4.87−4.77 (m, 4H), 4.58 (s, 4H), 4.18 (t, ^3J(H,H) = 8.0 Hz, 2H), 4.13 (d, ^3J(H,H) = 8.3 Hz, 2H), 4.09−4.05 (m, 4H), 3.93 (dd, ^3J(H,H) = 11.3, 6.1 Hz, 2H), 3.78−3.73 (m, 6H), 3.72−3.60 (m, 15H), 3.55 (d, ^3J(H,H) = 3.8 Hz, 3H), 3.51 (dd, ^3J(H,H) = 10.2, 3.2 Hz, 2H), 3.48 (dd, ^3J(H,H) = 9.9, 3.4 Hz, 2H), 2.60 (s, 2H), 2.56 (s, 2H), 1.08 ppm (s, 6H); ^{13}C NMR (125 MHz, [D$_4$]methanol): δ = 171.2, 158.2, 150.8, 145.8, 140.2, 131.0, 126.5, 125.3, 121.9, 115.3, 114.5, 113.1, 105.9, 101.1, 93.6, 81.6, 78.8, 77.7, 75.5, 74.5, 73.6, 73.0, 72.1, 70.9, 70.2, 69.4, 69.1, 65.0, 63.6, 62.8, 54.7, 52.0, 44.0, 40.0, 32.9, 28.2 ppm. IR (KBr): ν = 2214 (ν_{CN}), 3415 (ν_{OH})

dx.doi.org/10.1021/bc500047r | *Bioconjugate Chem.* 2014, 25, 773−787

cm^{-1}; HRMS (EI+): m/z calculated for $C_{65}H_{94}N_9O_{32}$: 1512.5999; found: 1512.5942.

Ethical Approval. Experiments were performed on 5−8-week-old male OF1 mice (Charles River Laboratories, L'Arbresle, France). All experiments and procedures were in accordance with the guidelines of the French Ministry of Agriculture (87/848) and of the European Community (86/609/EEC). They were approved by the local animal ethic committee of Rhône-Alpes, approval numbers 692660602, 0292.

Isolation of Single FDB Fibers. Single muscle fibers were isolated from the mouse Flexor Digitorum Brevis as previously described.[24] In brief, mice were killed by cervical dislocation. Muscles were isolated and placed in a Tyrode solution containing 0.2% collagenase (Sigma, type 1) for 50 min at 37 °C. After this treatment, muscles were kept in Tyrode at 4 °C and used within 12 h. Single fibers were obtained by triturating the muscles within the experimental chamber. For imaging, fibers were bathed in Tyrode.

Solution and Probes. Tyrode solution contained (in mM): 136 NaCl, 5 KCl, 2.6 $CaCl_2$, 1 $MgCl_2$, 10 Hepes, 10 Glucose, 5 Pyruvate. All chemicals were purchased from Sigma (St. Louis, MO, USA). Di-4-ANEPPS, Di-8-ANEPPS, and ER Tracker Green were purchased from Molecular Probes (Eugene, OR, USA). Loading of the probes was carried out at room temperature in Tyrode. Stock solutions were made in DMSO, such that the final concentration of DMSO in experimental chamber was always below 1/1000 (except for compound **18** and **19**).

Confocal Imaging. Imaging was performed at room temperature using a Zeiss LSM 5 Exciter laser scanning confocal microscope (Zeiss, Jena, Germany) equipped with a 63× oil immersion objective, numerical aperture 1.4. The excitation was provided by an argon laser (488 nm) and fluorescence was collected above 650 nm with adjusting the PMT gain. Fibers were imaged in full frame (xy) mode. The zoom factor was set to either 1× or 2× corresponding to a xy pixel size of 200 or 100 nm, respectively. Frame size was 512 × 512 pixels, with a pixel depth of 12 bits. Pinhole was set to 1 airy unit. Spectral imaging was performed using a Zeiss LSM 710 available at the PLATIM, IFR 128 BiosSciences Gerland-Lyon Sud. Excitation was provided by an argon laser (488 nm) and emission was collected between 549 and 725 nm, with 9 nm incremental steps. The pixel depth was set to 8 bits. Image and data processing were performed using ImageJ (NIH, USA) and Microcal Origin (Microcal Software Inc., Northampton, MA, USA). To compare the specificity of the staining, only the brightness of the displayed pictures was adjusted. For the fluorescence intensity profile, the values are given before brightness correction.

■ ASSOCIATED CONTENT

Supporting Information

Materials and methods for Langmuir measurement and Brewster angles microscopy, additional figures including confocal images, general information for synthesis, and complete ^1H and ^{13}C NMR data for all compounds. This material is available free of charge via the Internet at http://pubs.acs.org.

■ AUTHOR INFORMATION

Corresponding Authors

*E-mail: yann.bretonniere@ens-lyon.fr.
*E-mail: stephane.chambert@insa-lyon.fr.

Present Address

Sandrine Pouvreau, Interdisciplinary Institute for Neuroscience, University of Bordeaux, CNRS UMR 5297, 33000 Bordeaux, France.

Author Contributions

The manuscript was written through contributions of all authors. All authors have given approval to the final version of the manuscript.

Notes

The authors declare no competing financial interest.

■ ACKNOWLEDGMENTS

We thank the ANR for financial support of this work and for a grant to S.R. (ANR-09-JCJC-0077-01), and the Région Rhône-Alpes for financial support and a grant to J.M.

■ REFERENCES

(1) Kobayashi, H., Ogawa, M., Alford, R., Choyke, P. L., and Urano, Y. (2010) New strategies for fluorescent probe design in medical diagnostic imaging. *Chem. Rev. 110*, 2620−2640.

(2) Lavis, L. D., and Raines, R. T. (2008) Bright ideas for chemical biology. *ACS Chem. Biol. 3*, 142−155.

(3) Przybylo, M., Borowik, T., and Langner, M. (2010) Fluorescence techniques for determination of the membrane potentials in high throughput screening. *J. Fluoresc. 20*, 1139−1157.

(4) Fluhler, E., Burnham, V. G., and Loew, L. M. (1985) Spectra, membrane-binding, and potentiometric responses of new charge shift probes. *Biochemistry 24*, 5749−5755.

(5) Jurkiewicz, P., Sykora, J., Olzynska, A., Humplickova, J., and Hof, M. (2005) Solvent relaxation in phospholipid bilayers: Principles and recent applications. *J. Fluoresc. 15*, 883−894.

(6) Jurkiewicz, P., Cwiklik, L., Jungwirth, P., and Hof, M. (2012) Lipid hydration and mobility: An interplay between fluorescence solvent relaxation experiments and molecular dynamics simulations. *Biochimie 94*, 26−32.

(7) Sanchez, S. A., Tricerri, M. A., and Gratton, E. (2012) Laurdan generalized polarization fluctuations measures membrane packing micro-heterogeneity in vivo. *Proc. Natl. Acad. Sci. U. S. A. 109*, 7314−7319.

(8) Bradley, J., Luo, R., Otis, T. S., and DiGregorio, D. A. (2009) Submillisecond optical reporting of membrane potential in-situ using a neuronal tracer dye. *J. Neurosci. 29*, 9197−9209.

(9) Clarke, R. J., and Kane, D. J. (1997) Optical detection of membrane dipole potential: Avoidance of fluidity and dye-induced effects. *Biochim. Biophys. Acta – Biomembranes 1323*, 223−239.

(10) Loew, L. M., Cohen, L. B., Salzberg, B. M., Obaid, A. L., and Bezanilla, F. (1985) Charge-shift probes of membrane-potential - Characterization of aminostyrilpyridinium dyes on the squid giant-axon. *Biophys. J. 47*, 71−77.

(11) Malkov, D. Y., and Sokolov, V. S. (1996) Fluorescent styryl dyes of the RH series affect a potential drop on the membrane/solution boundary. *Biochim. Biophys. Acta – Biomembranes 1278*, 197−204.

(12) Kolter, T., and Sandhoff, K. (1999) Sphingolipids - Their metabolic pathways and the pathobiochemistry of neurodegenerative diseases. *Angew. Chem., Int. Ed. 38*, 1532−1568.

(13) Fyrner, T., Magnusson, K., Nilsson, K. P. R., Hammarström, P., Aili, D., and Konradsson, P. (2012) Derivatization of a bioorthogonal protected trisaccharide linker toward multimodal tools for chemical biology. *Bioconjugate Chem. 23*, 1333−1340.

(14) Reeve, J. E., Anderson, H. L., and Clays, K. (2010) Dyes for biological second harmonic generation imaging. *Phys. Chem. Chem. Phys. 12*, 13484−13498.

(15) Campagnola, P. J., Wei, M. D., Lewis, A., and Loew, L. M. (1999) High-resolution nonlinear optical imaging of live cells by second harmonic generation. *Biophys. J. 77*, 3341−3349.

(16) Moreaux, L., Sandre, O., Charpak, S., Blanchard-Desce, M., and Mertz, J. (2001) Coherent scattering in multi-harmonic light microscopy. *Biophys. J. 80*, 1568−1574.
(17) Barsu, C., Cheaib, R., Chambert, S., Queneau, Y., Maury, O., Cottet, D., Wege, H., Douady, J., Bretonnière, Y., and Andraud, C. (2010) Neutral push-pull chromophores for nonlinear optical imaging of cell membranes. *Org. Biomol. Chem. 8*, 142−150.
(18) Shynkar, V. V., Klymchenko, A. S., Kunzelmann, C., Duportail, G., Muller, C. D., Demchenko, A. P., Freyssinet, J.-M., and Mely, Y. (2007) Fluorescent biomembrane probe for ratiometric detection of apoptosis. *J. Am. Chem. Soc. 129*, 2187−2193.
(19) Kim, H. M., Choo, H.-J., Jung, S.-Y., Ko, Y.-G., Park, W.-H., Jeon, S.-J., Kim, C. H., Joo, T., and Cho, B. R. (2007) A two-photon fluorescent probe for lipid raft imaging: C-Laurdan. *ChemBioChem 8*, 553−559.
(20) Kim, H. M., Jeong, B. H., Hyon, J.-Y., An, M. J., Seo, M. S., Hong, J. H., Lee, K. J., Kim, C. H., Joo, T., Hong, S.-C., and Cho, B. R. (2008) Two-photon fluorescent turn-on probe for lipid rafts in live cell and tissue. *J. Am. Chem. Soc. 130*, 4246−4247.
(21) Kucherak, O. A., Oncul, S., Darwich, Z., Yushchenko, D. A., Arntz, Y., Didier, P., Mély, Y., and Klymchenko, A. S. (2010) Switchable nile red-based probe for cholesterol and lipid order at the outer leaflet of biomembranes. *J. Am. Chem. Soc. 132*, 4907−4916.
(22) Xu, C., Zipfel, W., Shear, J. B., Williams, R. M., and Webb, W. W. (1996) Multiphoton fluorescence excitation: New spectral windows for biological nonlinear microscopy. *Proc. Natl. Acad. Sci. U. S. A. 93*, 10763−10768.
(23) Besset, C., Chambert, S., Fenet, B., and Queneau, Y. (2009) Direct azidation of unprotected carbohydrates under Mitsunobu conditions using hydrazoic acid. *Tetrahedron Lett. 50*, 7043−7047.
(24) Pouvreau, S. (2010) Superoxide flashes in mouse skeletal muscle are produced by discrete arrays of active mitochondria operating coherently. *PLoS ONE 5*.
(25) Lemke, R. (1974) Knovenagel condensations in dimethylformamide. *Synthesis-Stuttgart*, 359−361.
(26) Massin, J., Dayoub, W., Mulatier, J. C., Aronica, C., Bretonnière, Y., and Andraud, C. (2011) Near-infrared solid-state emitters based on isophorone: synthesis, crystal structure and spectroscopic properties. *Chem. Mater. 23*, 862−873.
(27) Massin, J., Charaf-Eddin, A., Appaix, F., Bretonnière, Y., Jacquemin, D., van der Sanden, B., Monnereau, C., and Andraud, C. (2013) A water soluble probe with near infrared two-photon absorption and polarity-induced fluorescence for cerebral vascular imaging. *Chem. Sci. 4*, 2833−2843.
(28) Dallmann, A., El-Sagheer, A. H., Dehmel, L., Mugge, C., Griesinger, C., Ernsting, N. P., and Brown, T. (2011) Structure and dynamics of triazole-linked DNA: biocompatibility explained. *Chem.—Eur. J. 17*, 14714−14717.
(29) Thirumurugan, P., Matosiuk, D., and Jozwiak, K. (2013) Click chemistry for drug development and diverse chemical−biology applications. *Chem. Rev. 113*, 4905−4979.
(30) Kolb, H. C., Finn, M. G., and Sharpless, K. B. (2001) Click chemistry: diverse chemical function from a few good reactions. *Angew. Chem., Int. Ed. 40*, 2004−2011.
(31) Rostovtsev, V. V., Green, L. G., Fokin, V. V., and Sharpless, K. B. (2002) A stepwise Huisgen cycloaddition process: Copper(I)-catalyzed regioselective "ligation" of azides and terminal alkynes. *Angew. Chem., Int. Ed. 41*, 2596−2599.
(32) Cecioni, S., Praly, J. P., Matthews, S. E., Wimmerova, M., Imberty, A., and Vidal, S. (2012) Rational design and synthesis of optimized glycoclusters for multivalent lectin-carbohydrate interactions: influence of the linker arm. *Chem.—Eur. J. 18*, 6250−6263.
(33) Garcia, G., Naud-Martin, D., Carrez, D., Croisy, A., and Maillard, P. (2011) Microwave-mediated 'click-chemistry' synthesis of glycoporphyrin derivatives and in vitro photocytotoxicity for application in photodynamic therapy. *Tetrahedron 67*, 4924−4932.
(34) Perez-Balderas, F., Ortega-Munoz, M., Morales-Sanfrutos, J., Hernandez-Mateo, F., Calvo-Flores, F. G., Calvo-Asin, J. A., Isac-Garcia, J., and Santoyo-Gonzalez, F. (2003) Multivalent neoglycoconjugates by regiospecific cycloaddition of alkynes and azides using organic-soluble copper catalysts. *Org. Lett. 5*, 1951−1954.
(35) Sholto, A., and Ehrenberg, B. (2008) Hydrophobicity, topography in membranes and photosensitization of silicon phthalocyanines with axial ligands of varying lengths. *Photochem. Photobiol. Sci. 7*, 344−351.
(36) Queneau, Y., Dumoulin, F., Cheaib, R., Chambert, S., Andraud, C., Bretonniere, Y., Blum, L. J., Boullanger, P., and Girard-Egrot, A. (2011) Two-dimensional supramolecular assemblies involving neoglycoplipids: Self-organization and insertion properties into Langmuir monolayers. *Biochimie 93*, 101−112.
(37) Glomm, W. R., Volden, S., Halskau, O., and Ese, M. H. G. (2009) Same system-different results: the importance of protein. Introduction protocols in Langmuir-monolayer studies of lipid-protein interactions. *Anal. Chem. 81*, 3042−3050.
(38) Guillemin, Y., Lopez, J., Gimenez, D., Fuertes, G., Valero, J. G., Blum, L., Gonzalo, P., Salgado, J., Girard-Egrot, A., and Aouacheria, A. (2010) Active fragments from pro- and antiapoptotic BCL-2 proteins have distinct membrane behavior reflecting their functional divergence. *PLoS ONE 5*.
(39) Stella, L., Mazzuca, C., Venanzi, M., Palleschi, A., Didonè, M., Formaggio, F., Toniolo, C., and Pispisa, B. (2004) Aggregation and water-membrane partition as major determinants of the activity of the antibiotic peptide Trichogin GA IV. *Biophys. J. 86*, 936−945.
(40) Brockman, H. (1999) Lipid monolayers: why use half a membrane to characterize protein-membrane interactions? *Curr. Opin. Struct. Biol 9*, 438−443.
(41) Verger, R., and Pattus, F. (1982) Lipid-protein interactions in monolayers. *Chem. Phys. Lipids 30*, 189−227.
(42) Maggio, B., Bianco, I. D., Montich, G. G., Fidelio, G. D., and Yu, R. K. (1994) Regulation by gangliosides and sulfatides of phospholipase A2 activity against dipalmitoyl- and dilauroylphosphatidylcholine in small unilamellar bilayer vesicles and mixed monolayers. *Biochim. Biophys. Acta – Biomembranes 1190*, 137−148.
(43) Girard-Egrot, A., Chauvet, J.-P., Gillet, G., and Moradi-Améli, M. (2004) Specific interaction of the antiapoptotic protein Nr-13 with phospholipid monolayers is prevented by the BH3 domain of Bax. *J. Mol. Biol. 335*, 321−331.
(44) Marsh, D. (1996) Lateral pressure in membranes. *Biochim. Biophys. Acta – Biomembranes 1286*, 183−223.
(45) Boisselier, E., Calvez, P., Demers, E., Cantin, L., and Salesse, C. (2012) Influence of the physical state of phospholipid monolayers on protein binding. *Langmuir 28*, 9680−9688.
(46) Calvez, P., Demers, E., Boisselier, E., and Salesse, C. (2011) Analysis of the contribution of saturated and polyunsaturated phospholipid monolayers to the binding of proteins. *Langmuir 27*, 1373−1379.
(47) Krol, S., Ross, M., Sieber, M., Kunneke, S., Galla, H. J., and Janshoff, A. (2000) Formation of three-dimensional protein-lipid aggregates in monolayer films induced by surfactant protein B. *Biophys. J. 79*, 904−918.
(48) Vollhardt, D. (1996) Morphology and phase behavior of monolayers. *Adv. Colloid Interface Sci. 64*, 143−171.
(49) Vollhardt, D., and Fainerman, V. B. (2000) Penetration of dissolved amphiphiles into two-dimensional aggregating lipid monolayers. *Adv. Colloid Interface Sci. 86*, 103−151.
(50) Rau, I., Armatys, P., Chollet, P. A., Kajzar, F., Bretonnière, Y., and Andraud, C. (2007) Aggregation: A new mechanism of relaxation of polar order in electro-optic polymers. *Chem. Phys. Lett. 442*, 329−333.